The Plant Cell, Vol. 27: 1547–1562, May 2015, www.plantcell.org

Two N-Terminal Acetyltransferases Antagonistically Regulate the Stability of a Nod-Like Receptor in Arabidopsis

Fang Xu,[a,b,1,2] Yan Huang,[a,b,c,2] Lin Li,[d,2] Patrick Gannon,[a,b] Eric Linster,[e] Monika Huber,[e] Paul Kapos,[a] Willy Bienvenut,[f] Bogdan Polevoda,[g] Thierry Meinnel,[f] Rüdiger Hell,[e] Carmela Giglione,[f] Yuelin Zhang,[b] Markus Wirtz,[e] She Chen,[d] and Xin Li[a,b,3]

[a] Michael Smith Laboratories, University of British Columbia, British Columbia V6T 1Z4, Canada
[b] Department of Botany, University of British Columbia, British Columbia V6T 1Z4, Canada
[c] College of Life Sciences, Sichuan Agricultural University, Ya'an, Sichuan 625000, PR China
[d] National Institute of Biological Sciences, Beijing 102206, PR China
[e] Centre for Organismal Studies, Heidelberg University, 69120 Heidelberg, Germany
[f] Institute for Integrative Biology of the Cell (I2BC), CEA, CNRS, University Paris-Sud, 91198 Gif sur Yvette Cedex, France
[g] University of Rochester, New York 14627

ORCID IDs: 0000-0003-0767-1272 (F.X.); 0000-0002-5226-2390 (Y.H.); 0000-0002-0743-4181 (B.P.); 0000-0001-5642-8637 (T.M.); 0000-0002-6238-4818 (R.H.); 0000-0001-7790-4022 (M.W.); 0000-0002-6354-2021 (X.L.)

Nod-like receptors (NLRs) serve as immune receptors in plants and animals. The stability of NLRs is tightly regulated, though its mechanism is not well understood. Here, we show the crucial impact of N-terminal acetylation on the turnover of one plant NLR, Suppressor of NPR1, Constitutive 1 (SNC1), in *Arabidopsis thaliana*. Genetic and biochemical analyses of SNC1 uncovered its multilayered regulation by different N-terminal acetyltransferase (Nat) complexes. SNC1 exhibits a few distinct N-terminal isoforms generated through alternative initiation and N-terminal acetylation. Its first Met is acetylated by N-terminal acetyltransferase complex A (NatA), while the second Met is acetylated by N-terminal acetyltransferase complex B (NatB). Unexpectedly, the NatA-mediated acetylation serves as a degradation signal, while NatB-mediated acetylation stabilizes the NLR protein, thus revealing antagonistic N-terminal acetylation of a single protein substrate. Moreover, NatA also contributes to the turnover of another NLR, RESISTANCE TO *P. syringae* pv *maculicola* 1. The intricate regulation of protein stability by Nats is speculated to provide flexibility for the target protein in maintaining its homeostasis.

INTRODUCTION

Protein regulation is of central importance to life. Protein synthesis is primarily regulated at the initiation stage, with evolutionarily conserved translation initiation and alternative translation initiation mechanisms. Recent global mapping of ribosome binding sites in mammals revealed that translation initiation is more versatile and alternative translation is more prevalent than previously imagined (Lee et al., 2012; Menschaert et al., 2013; Vanderperre et al., 2013; M.S. Kim et al., 2014; Van Damme et al., 2014; Wilhelm et al., 2014). Such mechanisms can vastly expand the diversity of the proteome and provide greater versatility for the encoded proteins.

Proteins perform diverse functions and their stability can vary drastically, with life spans ranging from one minute to several days (Belle et al., 2006; Yen et al., 2008). Thus, regulation of protein turnover is crucial for maintaining protein concentration and function. In eukaryotic organisms, protein stability is largely regulated through the ubiquitin proteasome system (UPS), which targets proteins modified with ubiquitin moieties (Vierstra, 2009; Weissman et al., 2011). Specificity of ubiquitination is primarily delivered by E3 ligases that specifically recognize the degradation signals (degrons) of their substrates. UPS-mediated proteolysis contributes broadly to the regulation of almost every biological process in eukaryotes.

Protein life span can be crudely estimated with a universal N-end rule, which is part of the UPS and relates the half-life of a protein with its N-terminal residues (Bachmair et al., 1986; Varshavsky, 2011; Tasaki et al., 2012). In eukaryotes, cotranslational N-terminal Met excision (NME) by Met aminopeptidases (MetAP) and N-α-terminal acetylation (Nt-acetylation) catalyzed by N-terminal acetyltransferases (Nats) are two major protein modifications contributing to the diversity of protein N termini and to the N-end rule (Giglione et al., 2000, 2003; Ross et al., 2005; Frottin et al., 2009; Gibbs et al., 2014a). Although limited studies have been conducted in plants on the N-end rule (Giglione et al., 2003; Graciet et al., 2009; Holman et al., 2009; Adam et al., 2011; Bienvenut et al., 2011; Gibbs et al., 2011, 2014b; Licausi et al., 2011; Weits et al., 2014), recent genomic and N-terminal acetylome analyses in yeast, animals, and plants revealed that the NME and Nt-acetylation processes, along with the related enzymatic activities, are largely conserved through eukaryotic lineages (Polevoda et al., 1999; Arnesen et al., 2009; Goetze et al., 2009; Bienvenut et al., 2012; Liu et al., 2013). Particularly, in vivo and in vitro studies have shown that all MetAPs share similar substrate specificity, removing the first Met only when

[1] Current address: Cold Spring Harbor Laboratory, Cold Spring Harbor, NY 11724.
[2] These authors contributed equally to this work.
[3] Address correspondence to xinli@msl.ubc.ca.
The author responsible for distribution of materials integral to the findings presented in this article in accordance with the policy described in the Instructions for Authors (www.plantcell.org) is: Xin Li (xinli@msl.ubc.ca).
www.plantcell.org/cgi/doi/10.1105/tpc.15.00173

the second residue has a small radius of gyration of the side chain; on the contrary, bulky amino acids do not allow the removal of the first Met (Bienvenut et al., 2012). These data have been used to model substrate specificity of MetAPs and build an efficient prediction tool (Termi*N*ator3; http://www.isv.cnrs-gif.fr/terminator3), predicting plant NME with greater than 96% accuracy (Martinez et al., 2008; Meinnel and Giglione, 2008; Bienvenut et al., 2012). Multicellular organisms tend to have more Nats and higher levels of Nt-acetylation. Among all the Nats identified (NatA to NatF), NatA is responsible for the majority of Nt-acetylation events (Starheim et al., 2012). NatA is highly conserved with respect to subunit composition and protein target specificity, although multicellular organisms seem to exhibit more complex subunit forms.

Although Nt-acetylation is one of the most common irreversible protein modifications in eukaryotes, its biological roles remain ambiguous. Since most accumulating proteins are N-terminally acetylated, Nt-acetylation has traditionally been hypothesized to protect proteins from degradation. However, recent studies on selected protein targets have revealed that depending on the specific protein substrates, Nt-acetylation can serve as signals for diverse functions including protein degradation, membrane targeting, and protein-protein interaction (Starheim et al., 2012). Interestingly, a more recent report also demonstrated that both unacetylated and acetylated proteins with Met as the first amino acid can be degraded by the Arg/N-end rule and Ac/N-end rule pathways, respectively (Hwang et al., 2010; Shemorry et al., 2013; H.K. Kim et al., 2014).

Nod-like receptors (NLRs) serve as immune receptors in plants and animals. Overaccumulation of NLRs often leads to autoimmunity, whereas insufficient NLRs can cause susceptibility to specific pathogens. Therefore, the stability of these receptors must be tightly regulated; however, the mechanisms influencing NLR stability are not well understood (Trujillo and Shirasu, 2010). Here, resulting from a forward genetic screen, we report the identification of *MUSE6*, which encodes the *Arabidopsis thaliana* ortholog of yeast Naa15, the auxiliary subunit of NatA. In NatA mutants, the protein level of NLR Suppressor of NPR1, Constitutive 1 (SNC1) is elevated, indicating that NatA contributes to SNC1 degradation and thus Nt-acetylation of SNC1 may act as a degron. NatA was also found to contribute to the turnover of RESISTANCE TO *P. Syringae* pv *maculicola* 1 (RPM1), another NLR protein. When the SNC1 N terminus was analyzed by mass spectrometry (MS) after immunopurification, we were amazed to find several distinct isoforms of SNC1. Considering its N-terminal amino acids are not substrates of MetAPs, these isoforms were most likely generated through alternative initiation. Two forms of Nt-acetylation were present for SNC1, with acetylation on either the first or the second Met. Only the second Met is acetylated in the *naa15-1* background, suggesting that NatA is only responsible for the acetylation of the first Met, which was found to serve as a degron. Acetylation of the first Met of SNC1 by NatA was also confirmed through in vitro studies. Surprisingly, the acetylation of the second Met, which is performed by NatB, operates as a stabilizing signal. Thus, a single protein can be targeted by different Nats, and Nats can coordinate with translation initiation and downstream machinery to ensure the production of proper forms of the polypeptide with proper life spans. Such complex regulation is speculated to help provide flexibility to the target protein and ensure appropriate functionality of the synthesized polypeptides under dynamic cellular conditions. Similar mechanisms may be particularly important during stress responses to ensure that proper concentrations of regulatory proteins are reached in a timely manner.

RESULTS

Characterization of the *muse6-1 mos4 snc1* Triple Mutant

NLR proteins feature a central nucleotide binding (NB) and a C-terminal leucine-rich repeat (LRR) domain (Maekawa et al., 2011; Dangl et al., 2013). In Arabidopsis, the *snc1* mutant carries a gain-of-function mutation between the NB and LRR domains of a Toll-interleukin 1 receptor (TIR)-type NLR, leading to constitutive defense responses and consequent dwarfism (Zhang et al., 2003). A single Glu-to-Lys amino acid change in snc1 renders the NLR protein more stable, leading to higher SNC1 accumulation in *snc1* (Cheng et al., 2011). These *snc1*-mediated autoimmune phenotypes are abolished in the presence of *modifier of snc1* (*mos*) mutations, genetic suppressors of *snc1* (Johnson et al., 2012). To search for negative regulators of NLR-mediated immunity, mutant, *snc1*-enhancing (*muse*) forward-genetic screens were performed to identify mutants enhancing *snc1*-associated phenotypes in *mos snc1* backgrounds (Huang et al., 2013). The *muse* screens have identified a number of regulatory components contributing to the turnover of SNC1 (S. Huang et al., 2014; Y. Huang et al., 2014). This article concerns the *muse6-1 mos4 snc1* triple mutant, isolated from an ethyl methanesulfonate-mutagenized *mos4 snc1* population (Palma et al., 2007; Huang et al., 2013).

As shown in Figure 1A, the *muse6-1 mos4 snc1* plant was much smaller than *mos4 snc1* and enhances the dwarfism of *snc1.* The expression of *PR-1* and *PR-2* defense marker genes was increased in the triple mutant plants (Figure 1B). When *muse6-1 mos4 snc1* seedlings were challenged with the virulent oomycete pathogen *Hyaloperonospora arabidopsidis* (*H.a.*) Noco2, *snc1*-like enhanced resistance was restored (Figure 1C). In addition, high SNC1 protein accumulation in *snc1* was restored in *muse6-1 mos4 snc1* (Figure 1D). Taken together, *muse6-1* enhances almost all aspects of *snc1*-associated autoimmunity in the *mos4 snc1* background.

Positional Cloning of *muse6-1*

To identify *muse6-1*, a positional cloning approach was used. Mutant *muse6-1 mos4 snc1* (in Columbia [Col] background) was crossed with Landsberg *erecta*, and the F1 plants were allowed to self-fertilize to generate the F2 mapping population. Through linkage analysis, the *muse6-1* mutation was eventually mapped between markers F5I6 #2 and F5I6 #4, a 90-kb region on chromosome 1 (Supplemental Figure 1A). To identify the *muse6-1* mutation, Illumina whole-genome sequencing was performed using nuclear DNA from *muse6-1 mos4 snc1* plants. Comparison between the mutant and the Arabidopsis reference genome sequence in the mapped region revealed only one candidate mutation. Direct Sanger Sequencing confirmed the G-to-A transition in *muse6-1 mos4 snc1*, occurring at the exon-intron boundary of the 15th intron of *At1g80410* (Supplemental Figure 1B).

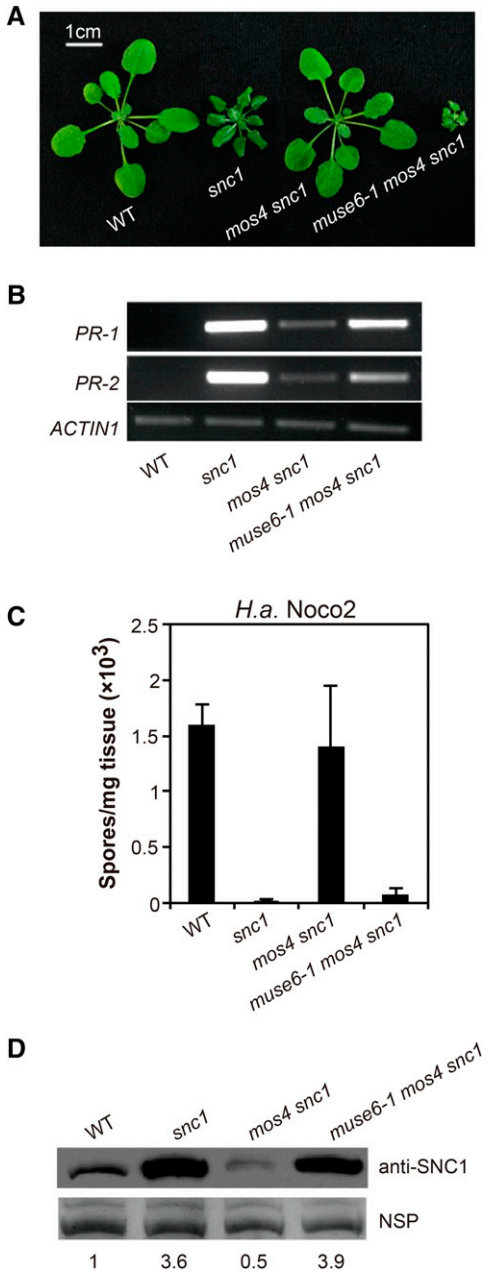

Figure 1. Characterization of the *muse6-1 mos4 snc1* Triple Mutant.

(A) Morphology of 3-week-old soil-grown Arabidopsis wild type (WT), *snc1*, *mos4 snc1*, and *muse6-1 mos4 snc1* plants.

(B) *PR-1* and *PR-2* gene expression in the indicated plants as determined by RT-PCR.

(C) Quantification of *H.a.* Noco2 sporulation on the indicated genotypes. Bars represent means of four replicates ± SD (n = 4 with 5 plants each).

(D) SNC1 protein levels in the indicated plants. Total protein was extracted from leaves of 4-week-old soil-grown plants. Proteins were separated on 8% SDS-PAGE gel and examined by immunoblot analysis with an anti-SNC1 antibody (Li et al., 2010). Ponceau staining signal of nonspecific proteins (NSPs) was used as an internal loading control. Image J was used to quantify the signal intensities of bands from SNC1 and NSPs. The signal intensity of SNC1 relative to NSP was calculated for each genotype and normalized to the value of the wild type, which is noted at the bottom of the image.

A *muse6-1* single mutant was isolated from the F2 population of a cross between *muse6-1 mos4 snc1* and wild-type Col plants by genotyping the *MUSE6*, *MOS4*, and *SNC1* loci. Comparison of the cDNA sequences between *muse6-1* and the wild type revealed a splicing pattern change in *muse6-1*; five extra nucleotides of the intron were spliced into the mRNA, introducing a premature stop codon and truncating the conserved NMDA receptor-regulated protein 1 domain of the encoded protein (Supplemental Figures 1C and 1D). Through RT-PCR, we found that the steady state transcript level of *MUSE6* is much lower in *muse6-1* than in wild-type plants (Supplemental Figure 1E), suggesting that the mRNA of *muse6-1* is less stable than the wild type, possibly due to nonsense-mediated decay, which is an mRNA surveillance mechanism that typically degrades transcripts with premature stop codons.

We also obtained an exonic T-DNA insertion allele of *muse6* (SAIL_688_G02), *muse6-2* (Supplemental Figure 1B). Among 48 plants sown on a Murashige and Skoog plate, no *muse6-2* homozygote was isolated. The *MUSE6/muse6-2* heterozygotes were wild-type like. Planting 32 progeny each from two independent plants that were heterozygous for the T-DNA insertion still did not yield any homozygotes. Among them, 22 and 24 plants were heterozygous for *muse6-2*, respectively, suggesting that homozygous *muse6-2* is lethal (expected ratio 2:1; $\chi^2 = 0.2$; $P > 0.05$). This is in agreement with an earlier report that mutation in *At1g80410* causes an embryo lethality phenotype (Johnston et al., 2007). To test whether *muse6-2* is allelic to *muse6-1*, a heterozygous *MUSE6/muse6-2* plant was crossed with homozygous *muse6-1 mos4 snc1* triple mutant. In F1, two types of plants were observed which segregated at a 1:1 ratio. Genotyping revealed that all the wild-type-like plants did not carry the T-DNA insertion, while all the dwarfed plants were heterozygous for *muse6-1* and *muse6-2* (Figure 2A), indicating that *muse6-2* failed to complement *muse6-1*, and *muse6-2* is allelic to *muse6-1*.

When MUSE6 protein was examined in *muse6-1* plants using an antibody specific to MUSE6 (Linster et al., 2015), minute amounts of wild-type MUSE6 protein could still be detected, suggesting that a small amount of normal mRNA of *MUSE6* is still produced in *muse6-1* plants (Supplemental Figure 1F). Taken together, these data indicate that *MUSE6* is *At1g80410*, and *muse6-2* is a null allele, while *muse6-1* is a partial loss-of-function allele.

To further confirm that *MUSE6* is *At1g80410*, wild-type *At1g80410* was cloned and transformed into *muse6-1* single mutant plants, which exhibit dwarf morphology and enhanced resistance to *H.a.* Noco2 (Figures 2B and 2C). All T1 plants reverted to wild-type stature (Figure 2B). When T2 plants were assayed with *H.a.* Noco2, the enhanced resistance in *muse6-1* was lost (Figure 2C), supporting that *At1g80410* fully complemented *muse6-1*, and *MUSE6* is indeed *At1g80410.* The homologs of *MUSE6* in human and yeast encode the auxiliary subunit Naa15 of NatA. In addition to the auxiliary subunit, NatA contains a catalytic subunit, Naa10 (Starheim et al., 2012). The catalytic subunit Naa10 of NatA in Arabidopsis is At5g13780, also known as At-NAA10. As with *NAA15*, loss of *NAA10* leads to lethality (Linster et al., 2015).

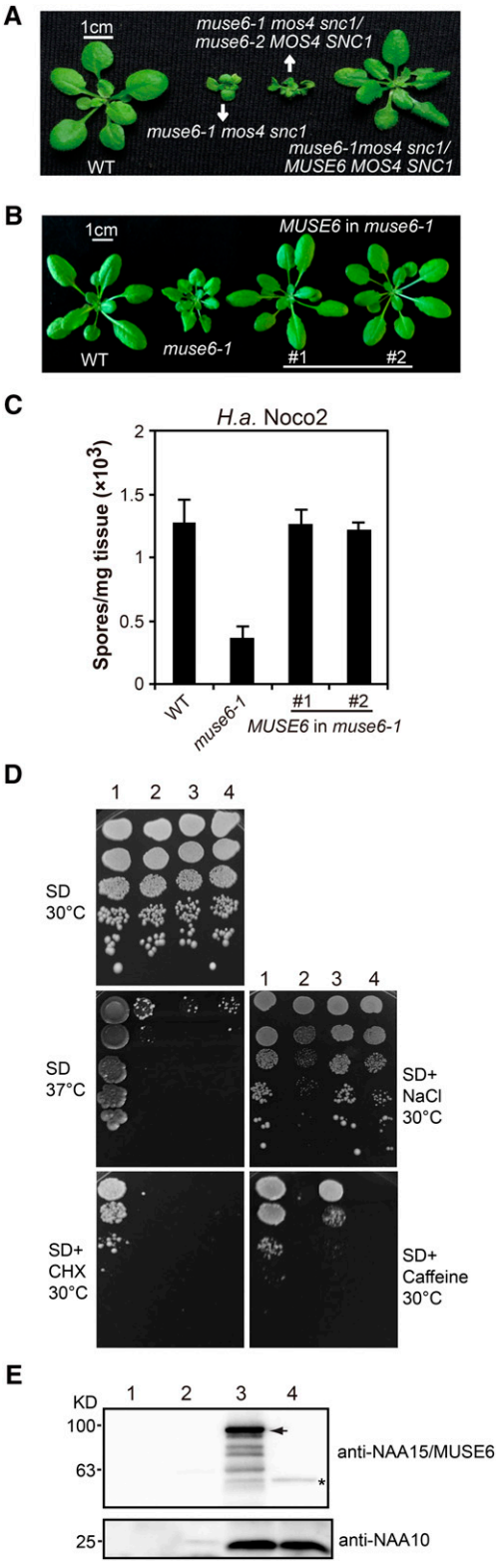

Figure 2. *MUSE6* Encodes the Auxiliary Subunit of NatA.

(A) Allelism test between *muse6-1* and heterozygous *muse6-2* (a T-DNA allele). Morphology of 3-week-old plants of wild-type, *muse6-1 mos4 snc1*, and two types of F1 plants from a cross between *muse6-1 mos4 snc1* and a heterozygous *muse6-2* plant. Homozygotes of *muse6-2* are not viable.

(B) Transgene complementation of *MUSE6* in *muse6-1*. Morphology of 4-week-old soil-grown plants of wild-type, *muse6-1*, and two representative transgenic lines expressing *MUSE6* under its native promoter in the *muse6-1* single mutant.

(C) Quantification of *H.a.* Noco2 sporulation on plants of the indicated genotypes. Bars represent means of four biological replicates ± SD ($n = 4$ with 5 plants each).

(D) Partial complementation of *S. cerevisiae naa15-Δ naa10-Δ* double mutant phenotypes by *MUSE6* and *NAA10*. The following yeast strains were grown to early log phase and the same number of cells were serially diluted (1/10) and spotted on the indicated medium: 1, wild type; 2, *naa15-Δ naa10-Δ* double mutant; 3, *naa15-Δ naa10-Δ* transformed with *MUSE6* and *NAA10*; and 4, *naa15-Δ naa10-Δ* transformed with *muse6-1* and *NAA10*. The plates were incubated at the indicated temperature with the corresponding medium: SD, synthetic defined premix of yeast minimal media; SD+CHX, SD with 0.18 μg/mL cycloheximide; SD+NaCl, SD with 1.15 M NaCl; SD+caffeine, SD with 0.11% caffeine.

(E) MUSE6, muse6-1, and NAA10 protein levels in the yeast lines used in **(D)**. Total protein samples were separated on 10% SDS-PAGE gel, and MUSE6 and muse6-1 were detected using anti-MUSE6 antibody, generated against the C terminus of NAA15/MUSE6 (Linster et al., 2015). NAA10 was detected by anti-NAA10, generated against the full-length NAA10 (Linster et al., 2015). The arrow indicates the normal MUSE6 protein, while the asterisk indicates a nonspecific signal from the muse6-1 protein when overexpressed in yeast. muse6-1 (1 to 463 of NAA15) is not detectable as the antibody is generated against the C-terminal residues 575 to 623 of NAA15.

Partial Complementation of Yeast *naa15-Δ naa10-Δ* Double Mutant by Arabidopsis *MUSE6* and *NAA10* Genes

To investigate the biological function of *MUSE6*, we performed a yeast complementation experiment. Previous studies on NatA complexes in human and yeast showed significant structural subunit differences between the species. Thus, we performed yeast complementation using a *naa15-Δ naa10-Δ* double mutant instead of a *naa15-Δ* single mutant. The yeast *naa15-Δ naa10-Δ* double mutant exhibits a number of defects, including temperature sensitivity and growth retardation on salt, caffeine, and cycloheximide-containing media (Arnesen et al., 2009). These defects are caused by a lack of N-acetylation of numerous proteins, including Orc1p (origin recognition complex 1 protein) and Sir3p (silence information regulator 1 protein) (Geissenhöner et al., 2004; Wang et al., 2004). The yeast expression vector pBEVY-U with a bidirectional promoter that directs constitutive expression of two different proteins at similar levels was used to express MUSE6 and NAA10 simultaneously (Miller et al., 1998). When *MUSE6* and *NAA10*, encoding the catalytic subunit of Arabidopsis NatA, were cotransformed into the yeast *naa15-Δ naa10-Δ* double mutant, they were not able to complement the heat sensitivity at 37°C, or the growth defect on cycloheximide-containing media (Figures 2D and 2E). However, *MUSE6* and *NAA10* could together fully complement the growth defect of *naa15-Δ naa10-Δ* on media containing NaCl and partially complemented on media containing caffeine. These data suggest that Arabidopsis MUSE6 and NAA10 are orthologous to the

yeast NatA complex, with some divergence. In addition, transformation of *muse6-1* together with *NAA10* partially complemented the growth defect of *naa15-Δ naa10-Δ* on media containing NaCl and was unable to complement the growth defect on media containing caffeine (Figures 2D and 2E). The partial complementation by *muse6-1* and *NAA10* corroborates that *muse6-1* is a partial loss-of-function allele. Since MUSE6 is orthologous to yeast Naa15, it is renamed as At-NAA15 to reflect its function. *muse6-1* is renamed as *naa15-1*, and *muse6-2* is renamed as *naa15-2*.

Characterizations of NatA Mutants

To better understand *NAA15*, we characterized the Arabidopsis *naa15-1/muse6-1* single mutant in detail. The mutant exhibits a unique dwarf morphology with slightly curled leaves (Figure 3A). With regards to immune phenotypes, *naa15-1* plants exhibit enhanced expression of both *PR-1* and *PR-2* (Figure 3B). Resistance to virulent *H.a.* Noco2 and bacteria *Pseudomonas syringae* pv *maculicola* (*P.s.m.*) ES4326 in *naa15-1* was significantly enhanced (Figures 3C and 3D). Interestingly, SNC1 protein levels were substantially higher in *naa15-1* plants compared with the wild type, whereas no detectable change in *SNC1* transcription was observed (Figures 3E to 3G), indicating that *naa15-1* affects the accumulation of SNC1 posttranscriptionally. Taken together, *naa15-1* plants exhibit autoimmunity and enhanced SNC1 accumulation.

To confirm the function of *NAA15* in plant immunity, we silenced *NAA15* in Arabidopsis using a microRNA-mediated approach. Two independent lines of *aminaa15* exhibiting different levels of silencing were selected (Linster et al., 2015). As shown in Supplemental Figure 2A, line *aminaa15* #2 with higher silencing resembles *naa15-1*, whereas the low silencing line *aminaa15* #1 is not distinguishable from the wild type except it is slightly smaller. More SNC1 accumulation and enhanced resistance to *H.a*. Noco2 were observed in these lines, correlating with the silencing levels (Supplemental Figures 2B and 2C). To further confirm the function of NatA in plant immunity, we also silenced the catalytic subunit of NatA, *NAA10*. Two independent lines of *aminaa10* were selected (Supplemental Figure 2A). The high silencing line *aminaa10 #23* also exhibited an *naa15-1*-like morphology, with high SNC1 accumulation and enhanced resistance to *H.a*. Noco2, whereas the low silencing line showed marginal effects in those aspects (Supplemental Figures 2B and 2C). These data corroborate the function of NatA in SNC1 accumulation and plant immunity.

Since the *naa15-1* single mutant exhibits enhanced immunity and heightened SNC1 accumulation, we investigated whether the autoimmunity of *naa15-1* is SNC1 dependent by examining *naa15-1 snc1-r1* double mutant plants, where *snc1-r1* is a loss-of-function allele of *SNC1* (Zhang et al., 2003). As shown in Supplemental Figure 2D, *naa15-1 snc1-r1* plants were morphologically *naa15-1*-like, but larger in size, indicating that *snc1-r1* partially suppresses the *naa15-1* phenotypes. The enhanced expression of *PR-1* and *PR-2* in *naa15-1* was also partially suppressed by *snc1-r1* (Supplemental Figure 2E). In addition, *snc1-r1* partially suppressed the enhanced resistance of *naa15-1* to *H.a.* Noco2 and *P.s.m*. ES4326 (Supplemental Figures 2F and 2G). Taken together, the enhanced immunity of *naa15-1* is partially dependent on SNC1, suggesting that SNC1 is an important, but not the only, target of NAA15.

SNC1 Protein Undergoes Alternative Initiation and Differential N-Terminal Acetylations

To test whether SNC1 is indeed acetylated at its N terminus, we attempted affinity purification of SNC1 protein using *SNC1-GFP* or *SNC1-HA* transgenic plants. Like other NLRs, SNC1 is of low abundance. The purity of SNC1 from one-step affinity purification was not suitable for MS analysis of its N terminus. Since FLAG-ZZ double tags were shown to be efficient tandem tags for affinity purification in an animal system (Knuesel et al., 2003), we constructed *SNC1-FLAG-ZZ* transgenic plants where genomic *SNC1* sequence was fused with C-terminal FLAG and ZZ tandem tags (Figure 4A). The fusion protein is fully functional as the *SNC1-FLAG-ZZ* overexpression transgenic plants showed autoimmune phenotypes with stunted growth, upregulation of *PR* gene expression, and enhanced resistance to *H.a.* Noco2 (Supplemental Figure 3). Tandem affinity purification enabled us to obtain sufficient SNC1 protein of high purity for MS analysis. Peptides detected by MS covered more than 50% of the full-length SNC1 sequence, with a single peptide being detected many times (Supplemental Figure 4A). This allowed us to quantitatively analyze the different SNC1 isoforms and modifications.

By comparing with the annotated SNC1 protein (At4g16890.1 in TAIR or AEE83820 in NCBI), the MS data revealed a number of novel details about SNC1. First, the second last intron of SNC1 annotated by TAIR turned out to be an exon, which encodes 127 extra amino acids (Supplemental Figure 4A). These data are consistent with a *SNC1* gene model experimentally verified by RT-PCR and 3′-rapid amplification of cDNA ends (Kim et al., 2010). Second, there is a 27-bp DNA sequence beginning with an in-frame start codon upstream of the annotated start codon by TAIR, which can encode an extra nine amino acids. Peptides beginning with these extra nine amino acids were detected in our MS data (Figure 4B; Supplemental Figure 4). In contrast, peptides starting with the annotated first Met were not detected, suggesting that the first Met was incorrectly predicted by TAIR. Interestingly, this extra peptide is unique to SNC1; it is not present in other TIR-NB-LRR NLR proteins (Supplemental Figure 5). Last, but most importantly, as shown in Figure 4B, different types of N-terminal modifications were detected, suggesting different protein isoforms.

Two possible nonexclusive hypotheses can explain the origin of the two SNC1 peptides starting at the first or second Met: (1) N-terminal MetAP processing by MetAP enzymes and/or (2) alternative initiation of the protein. As in other eukaryotes, plants have two types of MetAPs (MetAP1A, MetAP2A, and MetAP2B), shown to be interchangeable and to display the same substrate specificity as MetAPs occurring in other organisms (Giglione et al., 2000; Ross et al., 2005; Frottin et al., 2006). Considering the well-established, conserved rules of MetAP substrate cleavage, N-terminal methionine amino peptidase removal can be predicted for any protein with very strong probability using Termi*N*ator3 (http://www.isv.cnrs-gif.fr/terminator3). MetAP substrate cleavage is possible only when the second amino acid following the first Met is a nonbulky residue, leaving the N terminus of the mature protein with new residues, such as Ala, Cys, Gly, Pro, Ser, Thr, or Val, which in turn can then undergo further N-terminal modifications (Frottin et al., 2006; Martinez et al., 2008; Meinnel and Giglione, 2008). In line with this, proteins starting with bulky residues after

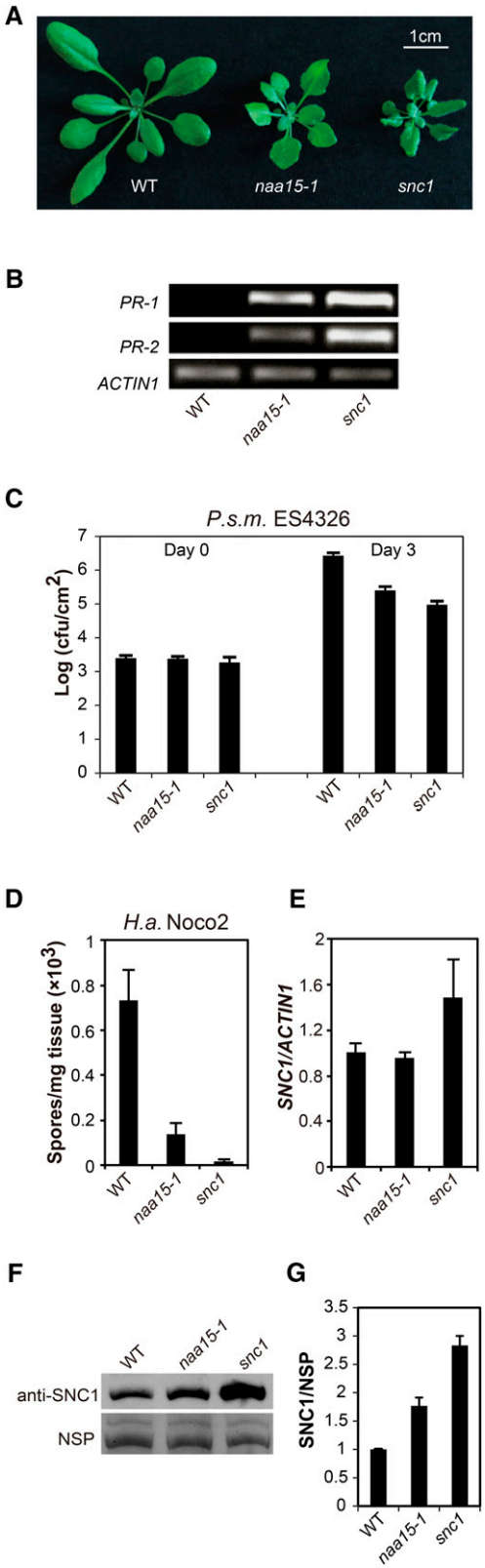

Figure 3. Characterization of the *naa15-1* Single Mutant.

the first Met, for example, another Met (as in the case with SNC1) or Asp, are not substrates of any MetAPs, and they will retain their first Met. In addition, the second Met of SNC1 is the more favorable start site because it has the optimal DNA context with both a purine at −3 and a guanine at the +4 position, whereas the first Met peptide has a purine at −3 and not a guanine at the +4 position (Kozak, 1991). Therefore, an alternative translation is the most likely explanation of the N-terminal peptide of SNC1 starting at the second Met.

NatA Specifically Acetylates the First Met of SNC1

To explore whether NatA is responsible for SNC1 acetylation, we examined SNC1-FLAG-ZZ in the *naa15-1* background. Interestingly, 100% of SNC1 detected in *naa15-1* plants started at the second Met and were all acetylated (Figure 4B). These data revealed two possible functions of NAA15. First, the complete disappearance of the acetylated first Met in *naa15-1* suggests that NAA15 as an auxiliary subunit of NAA10 in the NatA complex is involved in the acetylation of the first Met of SNC1. Since higher accumulation of SNC1 was observed in *naa15-1* plants, in which the acetylation on the first Met is abolished, this indicates that the acetylation of the first Met serves as a degron for the protein. Moreover, since the protein level of the only present form of SNC1 (i.e., with the second Met acetylated) in *naa15-1* mutant plants was augmented, this suggests that unlike the acetylation of the first Met by the NatA complex, the acetylation of the second Met of SNC1 by other Nat complexes might stabilize the protein in the *naa15-1* background.

To confirm that NatA specifically acetylates the first Met of SNC1, we performed in vitro enzymatic assays using the catalytic subunit of NatA, NAA10. Two peptides containing different SNC1 N termini were synthesized, with the first Met (SNC1 MM) or without (SNC1 M) (Figure 4C). The NAA10 protein had similar enzymatic activity on the SNC1 MM peptide (Figure 4D) as OASTL A: a peptide starting with a canonical NatA substrate, ASRIAK

(A) Morphology of 4-week-old soil-grown plants of the wild type, *naa15-1*, and *snc1*.

(B) *PR-1* and *PR-2* expression in the indicated plants as determined by RT-PCR.

(C) Growth of *P.s.m.* ES4326 in 4-week-old leaves of the wild type, *naa15-1*, and *snc1* at 0 and 3 d postinoculation, with bacterial inoculum of OD_{600} = 0.001. Bars represent means of five biological replicates ± SD.

(D) Quantification of *H.a.* Noco2 sporulation on 2-week-old plants of the indicated genotypes. Bars represent means of four biological replicates ± SD.

(E) *SNC1* expression level in 4-week-old soil-grown plants of the wild type, *naa15-1*, and *snc1* as determined by quantitative RT-PCR. Expressions were normalized to the wild type. Bars represent means of three technical replicates ± SD. The experiment was repeated three times with similar results.

(F) SNC1 protein levels in wild-type, *naa15-1*, and *snc1* plants. Similar experimental procedure was performed as in Figure 1D.

(G) The relative SNC1 protein level calculated from three independent experiments as described in **(F)**. The band intensity of SNC1 was analyzed as in Figure 1D. Bars represent means of three biological replicates ± SE.

A

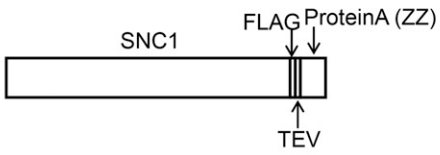

B

N-terminal a.a \ Genotype	*SNC1-FLAG -ZZ*	*SNC1-FLAG -ZZ naa15-1*
MMDTSKDDDMEIASSSGSR	7±4	0
Ac-MMDTSKDDDMEIASSSGSR	9±1	0
Ac-MDTSKDDDMEIASSSGSR	68±8	100±0
MDTSKDDDMEIASSSGSR	16±10	0

C

	Sequence
SNC1 MM	MMDTSKDDDMERWGRPVGRRRRPVRVYP
SNC1 M	MDTSKDDDMERWGRPVGRRRRPVRVYP
OAS-TL A	ASRIAKDVTERWGRPVGRRRRPVRVYP
Neg CTRL	SPTPPLFSLPRWGRPVGRRRRPVRVYP
SNC1 MAM	MAMDTSKDDDMERWGRPVGRRRRPVRVYP

D

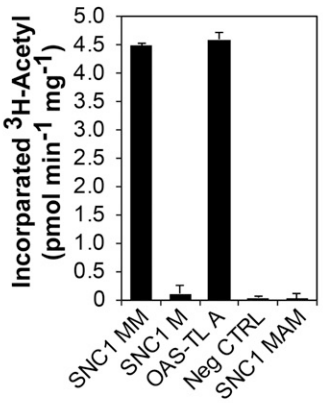

E

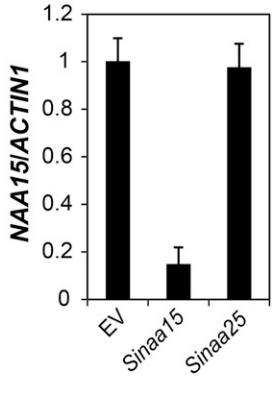

F

N-terminal a.a \ Genotype	EV	*Sinaa15*
MMDTSKDDDMEIASSSGSR	9±1	34±3
Ac-MMDTSKDDDMEIASSSGSR	39±1	22±3
Ac-MDTSKDDDMEIASSSGSR	52±1	44±5

Figure 4. The SNC1 Protein Undergoes Two Independent N-Terminal Acetylation Events, and the First Met of SNC1 Is Acetylated by NatA.

(Wirtz et al., 2010; Arnesen, 2011). However, NAA10 did not show any activity on SNC1 M or SNC1 MAM (an artificial N-terminal peptide of SNC1, which has an alanine residue inserted between the first two MM of SNC1), suggesting that NatA specifically acetylates the first Met, but not the second Met of SNC1.

To examine whether NatA specificity and alternative initiation of SNC1 is conserved in other plants, we tested whether NatA is also responsible for acetylation of the first Met of full-length SNC1 in *Nicotiana benthamiana*. When we performed immunoprecipitation-mass spectrometry (IP-MS) of SNC1-FLAG expressed in *N. benthamiana* in both the wild type and *Sinaa15*, a virus-induced gene silencing (VIGS) line targeting the *N. benthamiana* homolog of At-*NAA15* (Figure 4E; Supplemental Figure 6A; Bachan and Dinesh-Kumar, 2012), 75% of the SNC1 sequence could be detected by MS, with the N-terminal peptides of SNC1 hit over 100 times (Supplemental Figure 7). With this robust MS result, a statistically significant decrease in acetylation of the first Met from 39 to 22% was observed in *Sinaa15* plants (Figure 4F). As a result, the percentage of nonacetylated first Met of SNC1 increased considerably from 9 to 34% (Figure 4F), supporting the hypothesis that *N. benthamiana* NatA also acetylates the first Met of SNC1. Furthermore, alternative initiation of SNC1 was also found to be conserved in *N. benthamiana.* Taken together, these

(A) The schematic diagram of SNC1 with a tandem affinity purification tag. The genomic sequence of SNC1 excluding the stop codon was fused with the tandem affinity purification tag at the C terminus. The tag has three parts, with 3xFLAG peptides, a TEV enzyme cleavage site, and the IgG binding protein A epitope (ZZ).

(B) A summary of the N-terminal peptides of SNC1 detected by MS in *SNC1-FLAG-ZZ* and *SNC1-FLAG-ZZ naa15-1* plants. The immunoaffinity-purified samples of SNC1-FLAG-ZZ protein in *SNC1-FLAG-ZZ* and *SNC1-FLAG-ZZ naa15-1* plants were subjected to SDS-PAGE and silver staining to visualize the SNC1-FLAG bands, which were recovered from the gel and underwent trypsin digest and MS analysis. Four different isoforms of SNC1 N termini were detected. The percentage of each isoform was calculated by its hit number divided by the total peptide hit number (Supplemental Figure 4C). The numbers indicate the average percentages of the isoform from two independent experiments ± SE (the original data are presented in Supplemental Figures 4B and 4C).

(C) Peptides and their sequences used in the NatA enzymatic assay in **(D)**.

(D) NatA enzymatic activities on the peptides as listed in **(C)** using crude extract from *E. coli* expressing HIS-MBP-Naa10. OAS-TLA and NegCTRL serve as positive and negative controls, respectively (Wirtz et al., 2010; Arnesen, 2011). Bars represent means of three replicates ± SD.

(E) The expression level of Nb-*NAA15* in the indicated genotypes. *Sinaa15* or *Sinaa25* indicates *N. benthamiana* plants in which Nb-*NAA15* or Nb-*NAA25* was silenced using the VIGS approach (Bachan and Dinesh-Kumar, 2012). EV indicates wild-type *N. benthamiana* plants transformed with empty vector, which serves as a negative control. Bars represent means of three technical replicates ± SD.

(F) A summary of the N-terminal peptides of SNC1 detected by MS in the indicated *N. benthamiana* plants. The immunoaffinity-purified SNC1-FLAG protein recovered from the silver-stained gel underwent trypsin digest and MS analysis. The numbers indicate the average percentages of the isoforms from two independent experiments ± SE (the original data are presented in Supplemental Figures 7B and 7C).

data suggest a possible destabilization role of the acetylated first Met of SNC1 and the complementary stabilizing role of both nonacetylated first Met and acetylated second Met (Figures 4B and 4F).

NatB Specifically Acetylates the Second Met of SNC1

In human and yeast, NatB specifically acetylates Met followed by an Asp (Starheim et al., 2012). As the second Met in SNC1 is followed by Asp, we hypothesized that NatB might be responsible for its acetylation. To test this, the catalytic subunit of NatB, NAA20, was expressed in *Escherichia coli* and tested for its acetylation activity. As shown in Figure 5A, the SNC1 M N terminus was accepted as a substrate by NAA20, demonstrating that NatB is able to acetylate the second Met of SNC1.

To further characterize the substrate specificity of NatB for the second Met of SNC1, we employed VIGS in *N. benthamiana* and generated *Sinaa25* plants, where the auxiliary subunit of *NatB* in *N. benthamiana*, Nb-*NAA25*, was silenced (Figure 5B; Supplemental Figure 6B). As shown in Figure 5C, acetylation of the second Met was decreased in *Sinaa25* plants compared with control plants (empty vector). As a result, the percentage of non-acetylated second Met of SNC1 is substantially increased from 0 to 26% (Figure 5C) due to inefficient NatB activity, suggesting that NatB is responsible for the acetylation of the second Met of SNC1. Silencing Nb-*NAA25* also seems to alter the homeostasis of SNC1 isoforms, as less acetylation of the first Met was observed in *Sinaa25* plants. We also noted the appearance of the 5% novel N-terminal peptide DTSKDDDMEIASSSGSR in *Sinaa25* plants. Taking into account NME rules for which no excision of Met is expected in proteins starting with MD, we cannot conclude about the source or significance of this peptide. Nevertheless, we speculate that removal of this Met may be a consequence of increased proteolytic activity in the *Sinaa25* plants.

Acetylation of the Second Met of SNC1 Stabilizes the Protein

To investigate the function of NatB in plant immunity, we characterized available Arabidopsis knockout mutants of the two subunits of NatB, *naa20* and *naa25*, and the double mutant *naa20tnaa25* (*naa20* was named *tcu2-2*, while *naa25* was named *nbc-1* in Ferrández-Ayela et al., 2013). Unlike in the *naa15-1* mutant, neither stunted growth nor enhanced resistance to pathogens was observed in *naa20*, *naa25*, or double mutant *naa20 naa25* plants (Figures 5D and 5E). Interestingly, SNC1 protein in the single or double mutants accumulated less compared with the wild type (Figures 5F and 5G), while *SNC1* expression was not reduced (Figure 5H), suggesting that defects in the NatB complex lead to the degradation of SNC1. In addition, *naa25* is able to substantially suppress the autoimmune phenotypes of *snc1* as well as the heightened SNC1 protein levels, confirming that NatB complex contributes to SNC1-mediated defense responses by altering SNC1 stability (Figures 5I to 5K). As NatB acetylates the second Met of SNC1, we concluded that acetylation of the second Met of SNC1 stabilizes the protein; in other words, the absence of acetylation of the second Met destabilizes the protein. Since acetylation of the first Met of SNC1 by NatA serves as a degron, our results are in line with the low overall level of SNC1 found in *NatB* mutants, enlightening the opposite effects of different Nat complexes on the stability of the same protein.

Testing the Significance of Nt-Acetylation on Another NLR, RPM1

Since the enhanced immunity of *naa15-1* is only partially dependent on *SNC1*, we further tested the influence of *naa15-1* on the protein levels of another NLR protein, a coil-coiled-type NLR, RPM1. Using Termi*N*ator3, RPM1, starting with MA, is predicted to first go through NME and then N-terminally acetylation by NatA (Figure 6A; Supplemental Figure 8A; Starheim et al., 2012). As shown in Figures 6B and 6C, RPM1 accumulated significantly more in *naa15-1* plants than in the wild type, indicating that NatA likely also contributes to the turnover of RPM1 and the Nt-acetylation of RPM1 probably also serves as a degron. When NatA activity is reduced in *naa15-1*, RPM1 becomes more stable. Consistent with the heightened RPM1 protein levels, *naa15-1* exhibits enhanced resistance to bacterial pathogen *P.s.t. avrRPM1*, which can be specifically recognized by NLR protein RPM1 (Figure 6D). In contrast, *NatB* mutants *naa20*, *naa25*, and the *naa20 naa25* double mutant did not show any detectable difference compared with the wild type when challenged with *P.s.t. avrRPM1*, agreeing with the Termi*N*ator3 prediction that RPM1 is not a target of the NatB complex.

Testing Acetylation Status of SNC1 Variants with Different N-Terminal Sequences

To further investigate the important role of N-terminal sequence on SNC1 acetylation, we performed site-directed mutagenesis of SNC1, generating SNC1 variants with substitutions of the second Met or the third Asp. By expressing different variants of SNC1-FLAG-ZZ in *N. benthamiana* followed by IP-MS, we detected different acetylation patterns in these variants (Figure 7A), suggesting that the N-terminal amino acid sequences affect the acetylation patterns. When the second Met was substituted with G or A, the first Met was excised by MetAPs and all the peptides were acetylated on the second G or A, agreeing perfectly with the prediction from Termi*N*ator3 that such a start would lead to the excision of the first Met and acetylation of the second G or A. When the second M was substituted with F, multiple N-terminal isoforms were detected. In these cases, only a minority of the first Met could be excised by MetAPs probably because MF is not as favorable a substrate for MetAPs as MA or MG. In addition, only partial acetylation was detected on the first Met and peptides without the first Met cannot be acetylated. Substitution of the third residue D also affected the N-terminal peptide pattern. Substitution of the third D with G resulted in only two isoforms, whereas substitution with F lead to diverse N-terminal forms (Figure 7A). These mutagenesis data corroborate that the sequence of the first few amino acids of the protein determine its MetAP and Nt-acetylation patterns.

DISCUSSION

Protein homeostasis is essential for cell survival, especially during stress responses like abiotic perturbations and biotic pathogen infections. The mechanisms of protein homeostasis in cells remain

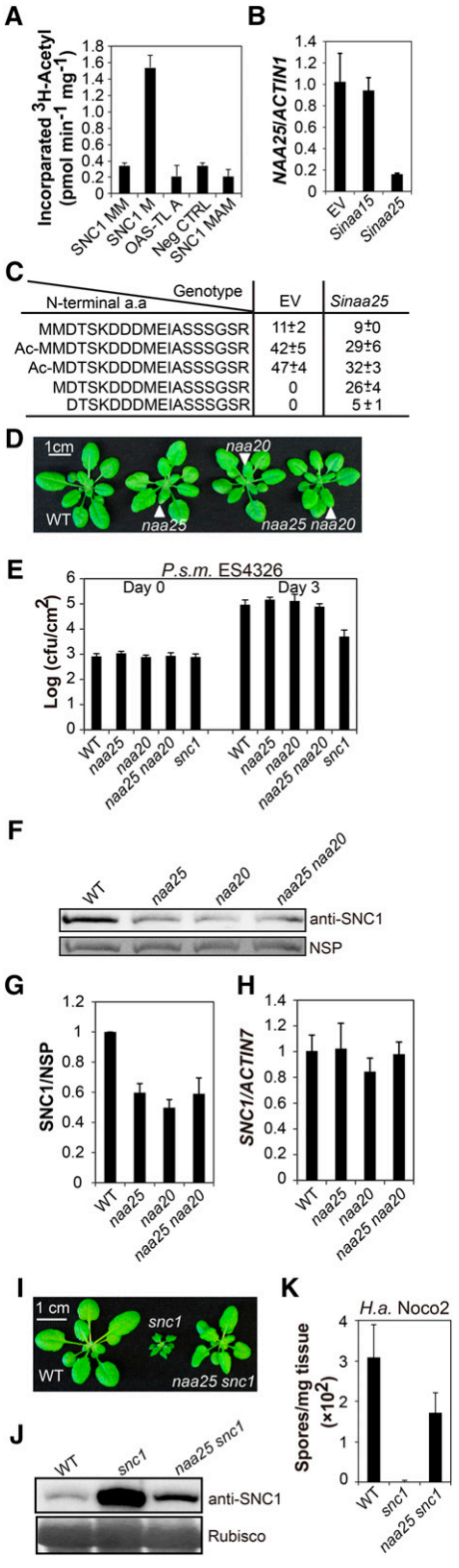

Figure 5. NatB Acetylates the Second Met of SNC1, Which Stabilizes the Protein.

largely unknown. Here, we report our functional studies of MUSE6, which was identified from a *snc1* enhancer screen in the *mos4 snc1* background. Our study reveals the unexpected, opposite effects of differential Nt-acetylation events on the stability of SNC1. The diverse isoforms of SNC1 offer an effective way of maintaining protein homeostasis (Figure 7B). Similar mechanisms regulating the turnover of important regulatory proteins in multicellular organisms can be envisioned.

Depending on the N terminus sequence, different proteins can be acetylated by specific Nat complex (Supplemental Figure 8A). Although most proteins are acetylated by NatA in yeast, depletion of the NatA complex only causes growth defects in special media or under high temperature stress (Arnesen et al., 2009; Figure 2D), indicating a nonessential function of NatA in yeast. However, in multicellular organisms, null alleles of *naa10* in *Drosophila melanogaster* and *naa15* in Arabidopsis are not viable (Wang et al., 2010; this study). Moreover, in humans, the Ser37Pro mutation in *Naa10* causes Ogden syndrome, a lethal X-linked disorder of male infants (Rope et al., 2011). Therefore, Nt-acetylation through NatA seems to be an essential mechanism for life in multicellular organisms, which is not surprising since NatA is the most prevalent Nat in metazoans (Starheim et al., 2012). In this study, we isolated a partial loss-of-function allele, *muse6-1/naa15-1*, from ethyl methanesulfonate mutagenesis. It enabled us to carry out genetic

(A) NatB enzymatic activities on the peptides as listed in Figure 4C using crude extract from *E. coli* expressing HIS-MBP-Naa20. Bars represent means of three replicates ± SD.

(B) The expression level of Nb-*NAA25* in the indicated *N. benthamiana* plants. The experiment was performed as in Figure 4E. Bars represent means of three technical replicates ± SD.

(C) A summary of the N-terminal peptides of SNC1 as detected by MS in the indicated *N. benthamiana* plants. Similar experimental procedures were performed as described in Figure 4F. The numbers indicate the average percentages of the isoforms from two independent experiments ± SE (the original data are presented in Supplemental Figures 7D and 7E).

(D) Morphology of 4-week-old soil-grown plants of the indicated genotypes.

(E) Bacterial growth of *P.s.m.* ES4326 on 4-week-old plants of the indicated genotypes at 0 and 3 d postinoculation, with bacterial inoculum at OD_{600} = 0.0005. Bars represent means of five replicates ± SD. *snc1* is used as a positive control.

(F) SNC1 protein levels in the indicated genotypes. The experiment was performed as described in Figure 1D.

(G) The relative SNC1 protein level as calculated from four independent experiments as described in **(E)**. The band intensity of SNC1 and NSP was analyzed as in Figure 3G. Bars represent means of four biological replicates ± SE.

(H) *SNC1* expression level in the indicated genotypes as determined by quantitative RT-PCR using a similar method as in Figure 3E. Bars represent means of three technical replicates ± SD. The experiment was repeated three times with similar results.

(I) Morphology of 4-week-old soil-grown plants of the wild type, *snc1*, and *naa25 snc1*.

(J) SNC1 protein levels in the indicated genotypes. The experiment was performed as described in Figure 1D.

(K) Quantification of *H.a.* Noco2 sporulation on plants of the indicated genotypes. Bars represent means of four biological replicates ± SD.

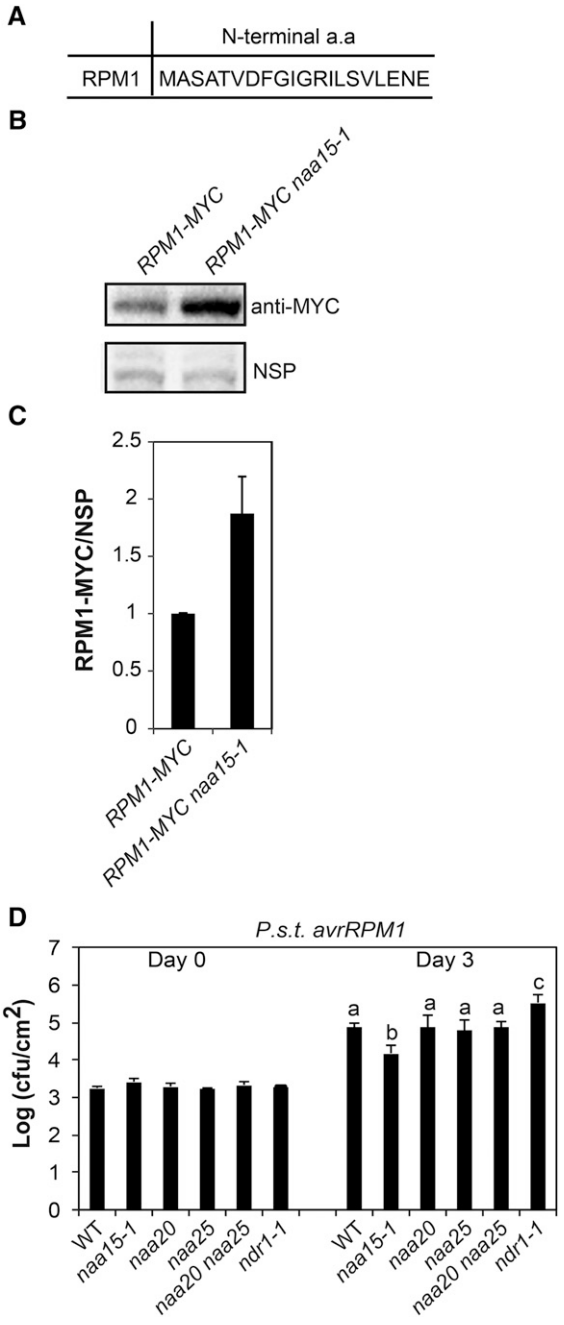

Figure 6. RPM1-MYC Protein Accumulates in *naa15-1* Plants.

(A) The N-terminal amino acid sequence of RPM1.

(B) RPM1-MYC protein levels in *RPM1-MYC* (Boyes et al., 1998) and *RPM1-MYC naa15-1* plants.

(C) The relative RPM1-MYC protein level in the indicated genotypes as analyzed from three biological replicates performed as in **(B)**. Bars represent means of three replicates ± SD. The band intensity of RPM1-MYC and NSP was quantified by ImageJ. For each genotype, the band intensity of RPM1-MYC was calculated relative to that of NSP. The values were then normalized to that of RPM1-MYC.

(D) Bacterial growth of *P.s.t.* avrRPM1 on 4-week-old plants of the indicated genotypes at 0 and 3 d postinoculation, with bacterial inoculum at OD_{600} = 0.001. *ndr1-1*, which is known to show enhanced susceptibility to *P.s.t. avrRPM1*, is used as a control (Aarts et al., 1998). Bars represent means of five replicates ± SD. Statistical analysis were performed by one-way ANOVA using StatsDirect. Statistically different groups are labeled by different letters ($P < 0.05$).

and molecular analysis on *NAA15* in plants. Although mutation in *muse6-1/naa15*-1 altered the gene splicing pattern, a small amount of wild-type naa15 protein can still be detected, suggesting that some wild-type *NAA15* mRNA is still produced, probably due to leaky splicing (Supplemental Figure 1F). In addition, naa15-1 together with the catalytic subunit NAA10 is able to partially complement the yeast NatA mutant, suggesting that the naa15-1 is partially functional (Figures 2D and 2E). Similar to NatA mutants, yeast NatB mutants are also viable with limited defects (Polevoda et al., 2003; Caesar et al., 2006). In opposition, NatB is essential for normal cell proliferation in human cells (Starheim et al., 2008). However, in Arabidopsis, although NatB mutants exhibit pleiotropic developmental phenotypes, their morphology and vigor are largely intact under regular lab growth conditions (Ferrández-Ayela et al., 2013; this study). This reflects a divergence in NatB between animal and plants, where plants seem to rely differently on NatB.

Due to a positive bias toward the occurrence of Nt-acetylation in the most abundant cytosolic proteins (Martinez et al., 2008), Nt-acetylation was long believed to stabilize proteins upon immediate synthesis of their N termini, preventing ubiquitination and further protein degradation (Hershko et al., 1984; Persson et al., 1985). However, N-terminally acetylated Ala, Val, Ser, Thr, or Cys, all of which are targets of NatA after first Met excision by MetAPs (Frottin et al., 2006), act as degrons in yeast and are targeted by the E3 ligase Doa10 for degradation (Hwang et al., 2010). Therefore, it was suggested that N-terminal acetylated degrons, which can be repressed via intramolecular folding or interactions with other proteins, may be dynamically exposed in vivo under specific conditions (Shemorry et al., 2013; H.K. Kim et al., 2014). Acetylation may play different roles on protein stability depending on its protein substrates, contributing to the homeostasis of the Nat targets.

In the case of SNC1, our data suggest that these seemingly contradictory hypotheses on Nats with opposite outcomes on protein stability can occur side by side on the same protein. Differential acetylations of SNC1 occur in both Arabidopsis and *N. benthamiana* (Figures 4 and 5), suggesting that the processes generating such isoforms are conserved. However, the acetylation pattern of SNC1 is slightly different in Arabidopsis than in *N. benthamiana* plants, likely reflecting the species difference in protein production (Figures 4 and 5). SNC1 starts with MMD. Two types of N termini, with either an MMD or an MD start, are generated probably through alternative initiations (Figures 4 and 5). These two forms are acetylated by different Nats (Figures 4, 5, and Figure 7), MMD by NatA and MD by NatB. Most interestingly, the acetylation of MMD serves as degron, while the acetylation of MD serves as a stabilizing signal for SNC1.

Why does one protein need to be regulated by different Nats with opposite effects? Since protein level depends on protein synthesis, which is mostly regulated at the initiation stage, using Nats to respond to cellular changes and meet cellular demands appears to be an ingenious mechanism to quickly generate proper

A

Genotype	N-terminal isoforms detected by MS	Number of MS Hit	Percentage
WT	MMDTSKDDDMEIASSSGSR	12	11
	Ac-MMDTSKDDDMEIASSSGSR	42	37
	Ac-MDTSKDDDMEIASSSGSR	59	52
M2G	Ac-GDTSKDDDMEIASSSGSR	90	100
M2A	Ac-ADTSKDDDMEIASSSGSR	63	100
M2F	MFDTSKDDDMEIASSSGSR	74	65
	Ac-MFDTSKDDDMEIASSSGSR	14	12
	FDTSKDDDMEIASSSGSR	25	22
D3G	MMGTSKDDDMEIASSSGSR	4	11
	Ac-MMGTSKDDDMEIASSSGSR	32	89
D3F	MMFTSKDDDMEIASSSGSR	17	17
	Ac-MMFTSKDDDMEIASSSGSR	16	15
	MFTSKDDDMEIASSSGSR	58	56
	Ac-MFTSKDDDMEIASSSGSR	12	11

B

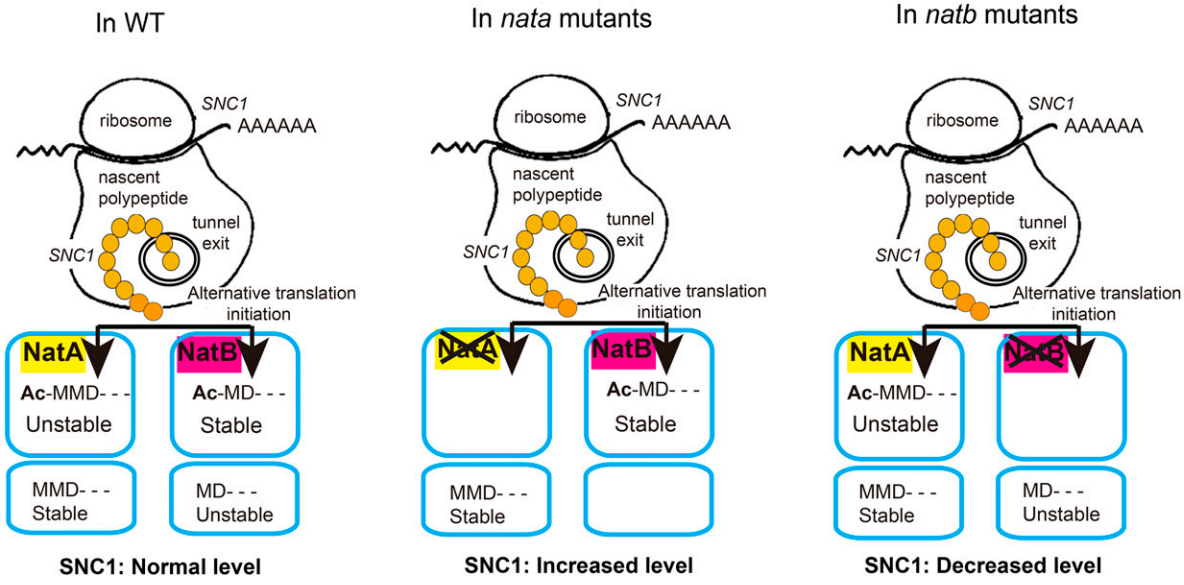

Figure 7. The N-Terminal Sequences of SNC1 Affect Its Acetylation Status and a Working Model on SNC1 N-Terminal Acetylation.

(A) MS analysis of different N-terminal site-mutagenized SNC1. The second M or the third D residue of SNC1 was substituted with the indicated amino acid by site mutagenesis approach. The primers used for site mutagenesis are included in Supplemental Table 1. Different variants were expressed in *N. benthamiana* followed by IP-MS; the hit numbers and percentages of different isoforms detected by MS for each SNC1 variant are shown.

(B) A working model on the different N-terminal acetylations of SNC1. In wild-type plants, SNC1 protein synthesis can be initiated at either the first or the second Met. The peptide translated from the first Met can be acetylated by NatA, which serves as a degron. The peptide translated from the second Met can be acetylated by NatB, where the protein is stabilized by the modification. SNC1 protein homeostasis is maintained by the coexistence of these different protein isoforms. In *nata* mutants, including *naa15-1*, *aminaa15*, and *aminaa10* plants, almost all the SNC1 peptides are acetylated at the second Met by NatB due to the inefficiency of NatA. The stabilization by acetylation on the second Met leads to increased SNC1 accumulation, partly leading to the autoimmune phenotypes of these plants. In *natb* plants, as a result of inefficient acetylation of the second Met of SNC1 by NatB that stabilizes the protein, the SNC1 protein level is decreased.

amounts of proteins. As differential Nt-acetylation might lead to protein isoforms with distinct stability, we speculate that different Nats may provide a faster solution to reach the appropriate concentration of target protein in the cell. Although SNC1 was shown to be acetylated and influenced by two different Nats, we wondered whether similar differential Nt-acetylations are rare. From the large proteomics analyses, which rarely catch low-abundance proteins, the identified abundant proteins (<15% of whole-proteome or acetylome) do not seem to exhibit differential acetylations (Arnesen et al., 2009; Goetze et al., 2009; Bienvenut et al., 2012; Liu et al.,

2013). It is possible that differential Nt-acetylations occur mostly on regulatory proteins whose levels need to be strictly regulated and are usually of very low abundance, such as proteins with MM starts like SNC1 (see below). Future work on specific regulatory proteins using efficient IP-MS approaches similar to ours will generate more N termini profiles to enrich our understanding on how Nt-acetylation regulates protein homeostasis.

What is special about proteins with MM starts? From whole-proteome or acetylome analysis, they are hardly ever found (Lee et al., 2012; Menschaert et al., 2013; Vanderperre et al., 2013; M.S. Kim et al., 2014; Van Damme et al., 2014; Wilhelm et al., 2014). However, when all 27,168 Arabidopsis proteins were analyzed, 620 were found to start with MM, representing over 2% of all encoded proteins. Our data on SNC1 suggest that the first Met of MM start proteins is targeted by NatA. The MM start also provides alternative initiation possibilities. Upon alternative initiation, the second Met can potentially be acetylated by a different Nat based on the residue at the third position (Supplemental Figure 8B). Lack of MM start proteins from proteomic data set indicates that they are of low abundance and perhaps with higher than average turnover rates. Agreeing with this prediction, the turnover of SNC1 is fast, with a half-life of about 2 h (Supplemental Figure 9), whereas the half-life of abundant plant proteins are over 24 h (Huffaker and Peterson, 1974). Therefore, proteins with an MM start may be more delicately regulated through both alternative initiation and Nt-acetylation, like SNC1, maintaining their fine-tuned concentrations.

How common is Nt-acetylation of NLRs? Among 152 NLRs surveyed in Arabidopsis, most are predicted to be targets of NatA, while some can be targeted by NatB, suggesting that Nt-acetylation plays important roles for many NLRs (Supplemental Figures 8C and 8D). As *naa15* mutants exhibit autoimmunity that is only partly dependent on SNC1 (Supplemental Figure 2), we suspect that NatA-mediated acetylation of other NLRs also contributes to their stability. Another possible target of NatA might be RPM1, as we detected heightened RPM1-MYC protein levels and enhanced RPM1-mediated defense responses in *naa15-1* plants (Figure 6). In addition, RPM1 is predicted to be acetylated by NatA, as it starts with MA, a typical substrate of NatA in eukaryotes post N-terminal Met excision (Starheim et al., 2012; Supplemental Figure 8A; Termi*N*ator3). Furthermore, only one other Arabidopsis NLR, AT1G27180, has an MM start. Therefore, it is unlikely that many NLRs have multiple N-terminal isoforms like SNC1. The diverse isoforms of SNC1 may enable more flexibility of the protein, making it a more sensitive sensor in response to pathogen stimuli.

Our results reveal the delicate regulation of NLR stability through N-terminal acetylation. The turnover of SNC1 and RPM1 is regulated through N-terminal acetylation. Differential initiation of SNC1 translation in combination with antagonistic N-terminal acetylations by different Nat complexes act as major contributors to SNC1 stability and the resulting immune response outputs. These findings support the recently proposed function of the ribosome as a central hub for protein quality control in eukaryotes (Pechmann et al., 2013) and provide a molecular explanation for the identification of *naa15-1/muse6-1* from an unbiased forward-genetics screen for stabilization of SNC1 in the *mos4 snc1* background. Our data strongly indicate that the N terminus of proteins is a hotspot for regulation of protein turnover in plants that might be tightly regulated in response to environmental stresses.

METHODS

Plant Growth Conditions and Pathogen Infections

All *Arabidopsis thaliana* and *Nicotiana benthamiana* plants were grown in climate-controlled chambers at 22°C under 16-h-light/8-h-dark cycles. The *muse* screen was described earlier (Huang et al., 2013). Infection experiments with *H.a.* Noco2 and *P.s.m.* ES4326 were performed as described previously (Zhang et al., 2003). The *naa15-1* single mutant was identified in the F2 of a cross between *muse6-1 mos4 snc1* and the wild type (Col) by genotyping *MUSE6*, *MOS4*, and *SNC1* loci using primers listed in Supplemental Table 1. The *naa15-1 snc1-r1* double mutant was obtained by crossing *naa15-1* with *snc1-r1* (Zhang et al., 2003), and the double mutant plants were identified in the F2 by genotyping. The *naa25 snc1* double mutant was obtained by crossing *naa25* with *snc1* (Zhang et al., 2003; Cheng et al., 2009), and the double mutant plants were identified in F2 by genotyping. The genotyping primers are detailed in Supplemental Table 1. Construction of *aminaa10* and *aminaa15* lines is described by Linster et al. (2015). All the mutant information is summarized in Supplemental Table 2.

Gene Expression Analysis

Gene expression analysis was performed as previously described by Y. Huang et al. (2014). Briefly, RNA was extracted using the Totally RNA kit (Ambion, now part of Invitrogen) from ~100 mg of plant tissues. Total RNA (0.4 μg) was used to reverse transcribe cDNA using Superscript II reverse transcriptase (Invitrogen), following the manufacturer's protocol. RT-PCR was performed using the QuantiFAST SYBR Green PCR kit (Qiagen). For *PR* gene expression, the cDNA was amplified by PCR using 94°C for 2 min and 28 cycles of 94°C for 20 s, 58°C for 30 s, and 68°C for 1 min. The products were subsequently analyzed by agarose gel electrophoresis and ethidium bromide staining. The primers for gene expression analyses used in this study are included in the Supplemental Table 1.

Protein Analysis

Total protein analysis was performed as described by Li et al. (2010). Briefly, ~100 mg plant tissues was ground in liquid N_2 to fine powder. Extraction buffer (100 mM Tris-HCl, 0.1% SDS, and β-mercaptoethanol) was added at 1:1 ratio to the powder and mixed well. The supernatant after centrifugation at 13,000 rpm was transferred to a new tube, mixed with 4× SDS loading buffer, and boiled at 95°C for 5 min. Proteins were separated on 8% SDS-PAGE gel and examined by immunoblot analysis with standard protein gel blotting protocol. For primary antibodies, anti-SNC1 (Li et al., 2010) was diluted at 1:400, anti-MYC (9E10; Santa Cruz) was diluted at 1:1000, anti-Flag (F3165; Sigma-Aldrich) was diluted at 1:5000, anti-NAA15 (Linster et al., 2015) was diluted at 1:400, and anti-NAA10 (Linster et al., 2015) was diluted at 1:400. For the secondary antibodies, both anti-mouse and anti-rabbit horseradish peroxidase-conjugated antibodies were diluted at 1:5000.

Construction of Plasmids

The *MUSE6* genomic sequence, plus 1.5-kb regions both upstream of the start codon and downstream of the stop codon, was amplified by primers MUSE6-KpnI-F and MUSE6-SalI-R (Supplemental Table 1) from wild-type genomic DNA. The amplified fragment was cloned into *pCAMBIA1305* to generate *pCAMBIA1305-pMUSE6:MUSE6*. The genomic DNA of *SNC1* without the stop codon plus the ~1.5-kb 5′-upstream promoter region was amplified by PCR with *Kpn*I and *Bam*HI sites separately introduced at the two primer ends. The fragment was cloned into a *pCambia1305-FLAG-ZZ* vector containing a C-terminal FLAG tag, TEV enzyme site, and ZZ tag. These constructs were electroporated into *Agrobacterium tumefaciens* and subsequently transformed into corresponding plants by floral dipping (Clough

and Bent, 1998). The transformants were selected on Murashige and Skoog plates with 30 μg/mL hygromycin. Full-length cDNAs of *NAA10* and *NAA20* were cloned into a pETM-41 vector (MBP/His-tag; Günter Stier, MPIMF Heidelberg, deposited in EMBL database) using the restriction sites *Acc65*I and *Nco*I for *NAA10* and *Bam*HI and *Nco*I for *NAA20*. Primers Naa10f and Naa10r were used for amplification of NAA10, and primers Naa20f and Naa20r were used for amplification of *NAA20*. The primer information is included in Supplemental Table 1.

Positional Cloning and Illumina Sequencing

Mutant *muse6-1 mos4 snc1* (in Col background) was crossed with Landsberg *erecta*, and the F1 plants were allowed to self-fertilize to generate the mapping population. Using 24 F2 plants with *snc1*-enhancing morphology as a crude mapping population, the *muse6-1* mutation was mapped to the bottom of chromosome 1 through linkage analysis. The mutation was further flanked between markers F28P22 and F23A5 using an additional 108 F2 plants that were obviously smaller than *snc1* (Figure 2A). A larger F3 fine mapping population was generated to further narrow down the molecular lesion. The F3 progeny were generated from several F2 lines that were heterozygous for the *muse6-1* mutation but homozygous at both *SNC1* (*snc1*) and *MOS4* (*mos4*) to avoid interference from *snc1* and *mos4*. Out of a 660 F3 progeny, 61 recombinants were collected between F28P22 and F23A5. The *muse6-1* mutation was eventually mapped between single nucleotide polymorphism markers F5I6 #2 (30.211 Mb) and F5I6 #4 (30.301 Mb), a distance of 90 kb, which was located on BAC clone F5I6 #6 (30.2338 Mb). The primer sequences are included in Supplemental Table 1. For Illumina sequencing, nuclear DNA was first isolated from *muse6-1 mos4 snc1* plants using the protocol described by Xu et al. (2012). The DNA was further purified using a standard CTAB DNA extraction protocol. A DNA library was then made according to the manufacturer's protocol (NEB Next Ultra DNA Library Prep Kit), which was followed by standard Illumina DNA sequencing.

Yeast Complementation

Yeast complementation was performed as described in Arnesen et al. (2009). Briefly, different yeast strains were cultured overnight in different liquid SD medium lacking the supplements that can be synthesized by the construct carried in the strains. The yeast stains were then reinoculated into fresh liquid medium and grown for another 4 to 6 h. When the cells grew to early log phase, they were counted under microscope and adjusted to the same concentration. The same number of cells were serially diluted (1/10) and spotted on the specific medium and cultured at 37°C or 30°C for 2 to 3 d for selection.

NAA10 and NAA20 in Vitro Enzymatic Assay

Escherichia coli Rosetta Star cells (DE3; Invitrogen), which harbor the pETM-41 vector containing the full-length *NAA10* or *NAA20* cDNA, were grown in Luria-Bertani medium at 37°C to an OD_{600} of 0.8. Expression of the NAA10 or the NAA20 protein fused via an N terminus to a histidine tag and a maltose binding protein HIS-MBP-NAA10 or HIS-MBP-NAA20 was triggered by addition of isopropyl β-D-1-thiogalactopyranoside (1 mM) for 5 h. Cells were harvested by centrifugation (10,000*g*, 4°C for 10 min) and lysed by sonication in lysis buffer (50 mM Tris-HCl, pH 7.5, 250 mM NaCl, 0.5 mM PMSF, and 20 mM imidazole). The crude protein extract was cleared by centrifugation at 28,000*g* at 4°C for 20 min and directly used in the enzymatic test system. Activity of crude protein extract of HIS-MBP-NAA10 or HIS-MBP-NAA20 (30 μg for total protein) was tested according to Evjenth et al. (2009) for 60 min at 37°C in acetylation buffer (50 mM Tris-HCl, pH 7.5, 10% glycerol, 10 mM DTT, and 1 mM EDTA) containing 500 μM [^{3}H] acetyl-CoA (7.48 GBq/mmol; Hartmann Analytics) and 0.2 mM peptide (Genecust). Peptide sequences are as follows: OAS-TL A, ASRIAKDVTERWGRPVGRRRRPVRVYP; SNC1 M, MDTSKDDDMERWGRPVGRRRRPVRVYP; SNC1 MM, MMDTSKDDDMERWGRPVGRRRRPVRVYP; SNC1 MAM, MAMDTSKDDDMERWGRPVGRRRRPVRVYP; and Neg CTRL, SPTPPLFSLPRWGRPVGRRRRPVRVYP.

Tandem Affinity Purification of SNC1

Immunoaffinity purification of SNC1-FLAG-ZZ was performed using modified protocols from Knuesel et al. (2003). ZZ tag produces an epitope of Protein A. About 80 g of plate-grown *SNC1-FLAG-ZZ* plants and 100 g of plate-grown *SNC1-GFP* plants, which served as the negative control, were harvested and ground in liquid nitrogen using a cold mortar and pestle. Each sample was homogenized in 120 mL lysis buffer (20 mM Tris-HCl, pH 7.4, 25% glycerol, 20 mM KCl, 2 mM EDTA, 2.5 mM $MgCl_2$, 250 mM sucrose, 1 mM DTT, 1 mM PMSF, and protease inhibitors) by incubation at 4°C for 30 min. The homogenates were then filtered through a 100- and 40-μm nylon mesh sequentially. The filtered homogenates were centrifuged at 1500*g* for 10 min to remove the precipitates. Triton X-100 was added into the supernatant to a final concentration of 0.2% to solubilize proteins. All the rest of the steps were performed at 4°C. After 30 min incubation at 4°C, the samples were first centrifuged at 16,000*g* for 15 min and centrifuged at 29,000*g* for another 15 min. The supernatants were incubated with 300 μL IgG beads (GE Healthcare) to pull down the ZZ tag (Protein A epitope) for 3 h. The beads were then pellet down by centrifuging at 4000 rpm for 5 min and washed three times with 15 mL wash buffer (20 mM HEPES-KOH, pH 7.9, 2.5 mM $MgCl_2$, 150 mM NaCl, 20% [v/v] glycerol, 0.2 mM EDTA, 0.2% Triton X-100, 1 mM DTT, 1 mM PMSF, and protease inhibitors), with 5 min incubation for each wash. The beads were washed with 10 mL TEV cleavage buffer (10 mM Tris-HCl, pH 8.0, 150 mM NaCl, 0.1% Nonidet P-40, 1 mM DTT, and 1 mM EDTA). The beads were incubated with 1 mL TEV cleavage buffer containing 3.5 μL TEV protease (AcTEV protease; Invitrogen) for 2 h and a second incubation with 500 μL TEV cleavage buffer with 1 μL TEV protease for 30 min. The supernatant was incubated with 60 μL anti-FLAG beads (Sigma-Aldrich) for 3 h. The beads were pelleted down by centrifugation at 8000 rpm for 1 min and washed eight times using 1 mL wash buffer. The proteins binding specifically to the beads were competitively eluted using 100 μL 250 μg/mL 3× FLAG peptides for 1 h. All the samples were boiled in SDS loading buffer for 5 min before running on SDS-PAGE gel. After silver staining of the gel using a kit from Sigma-Aldrich (PROTSIL2-1KT), the SNC1 band was recovered from the gel and destained using reagents in the silver staining kit.

VIGS in *N. benthamiana*

VIGS was performed as described by Bachan and Dinesh-Kumar (2012). Briefly, an ~500-bp fragment of *NAA15* or *NAA25* from *N. benthamiana* was amplified with PCR and cloned into VIGS vector *pTRV2*. The constructs were then transformed into Agrobacterium GV3101. The Agrobacterium containing the *pTRV2* constructs was mixed with Agrobacterium-containing VIGS vector *pTRV1* at 1:1 ratio and coinfiltrated into *N. benthamiana* leaves when the plants had two to four true leaves. After ~3 weeks, the expression of *NAA15* or *NAA25* was examined using real-time PCR. SNC1-FLAG was transiently expressed after validation of silencing of the target gene, following a protocol as described in Xu et al. (2014). The primers used for making the constructs and examining the gene expression are included in Supplemental Table 1.

MS Analysis

Protein bands on the SDS-PAGE gel were destained according to the manufacturer's protocol (PROTSIL2-1KT) and in-gel digested with sequencing grade trypsin (10 ng/μL trypsin and 50 mM ammonium bicarbonate, pH 8.0) overnight at 37°C. Peptides were extracted with 5% formic acid/50%

acetonitrile and 0.1% formic acid/75% acetonitrile sequentially and then concentrated to ~20 μL. The extracted peptides were separated by an analytical capillary column (50 μm × 15 cm) packed with 5 μm spherical C18 reversed phase material (YMC). A Waters nanoAcquity UPLC system was used to generate the following HPLC gradient: 0 to 30% B for 60 min and 30 to 70% B for 15 min (A = 0.1% formic acid in water, B = 0.1% formic acid in acetonitrile). The eluted peptides were assayed using a LTQ Orbitrap Velos mass spectrometer (Thermo Fisher Scientific) equipped with a nano-electrospray ionization source. The mass spectrometer was operated in data-dependent mode with one MS scan followed by four collision-induced dissociation and four high-energy collisional dissociation tandem MS scans for each cycle. Database searches were performed on an in-house Mascot server (Matrix Science) against experimental SNC1 protein sequence (Supplemental Figure 4). The search parameters were as follows: 7 ppm mass tolerance for precursor ions, 0.5 D mass tolerance for product ions, and three missed cleavage sites were allowed for trypsin digestion and semi-trypsin search model. The following variable modifications were included: oxidation on methionine, carbamidomethylation on cysteine, acetylation on lysine, acetylation on protein N terminus, and phosphorylation on serine, threonine, and tyrosine.

Cycloheximide Chase Experiment

Two-week-old plate-grown seedlings were submerged in liquid Murashige and Skoog containing 7.5 mM cycloheximide and 0.01% Silwet L-77 and vacuumed for 5 min before incubation for another 25 min at room temperature. Total protein was then extracted at different time points.

Accession Numbers

Sequence data of genes and vectors used in this article can be found in the GenBank/EMBL libraries under the following accession numbers: At5g13780 (*NAA10*), At1g03150 (*NAA20*), At5g58450 (*NAA25*), At4g16890 (*SNC1*), At3g18165 (*MOS4*), At1g80410 (*MUSE6*/*NAA15*), At3g07040 (*RPM1*), AF406991 (*pTRV2*), YL192 (*pTRV1*) AF069724.1 (*pBEVY-U*), and AF354045.1 (*pCAMBIA1305*).

Supplemental Data

Supplemental Figure 1. Positional Cloning of *muse6-1*.

Supplemental Figure 2. Characterization of the *NatA*-Silenced Mutants and *naa15-1 snc1-r1* Double Mutant.

Supplemental Figure 3. *SNC1-FLAG-ZZ* Transgenic Plants Exhibit Autoimmune Phenotypes That Can Be Enhanced in the *muse6-1* Background.

Supplemental Figure 4. The Original MS Data for Figure 4B.

Supplemental Figure 5. Amino Acid Alignments of the N Terminus of SNC1 with Its Homologs in Arabidopsis and *Nicotiana tabacum*.

Supplemental Figure 6. The Nat Protein Alignments between Arabidopsis and *N. benthamiana*.

Supplemental Figure 7. The Original MS Data for Figures 4F and 5C.

Supplemental Figure 8. Nat Target Protein Analyses.

Supplemental Figure 9. Measuring the Half-Life of SNC1.

Supplemental Table 1. Summary of the Primers Used in the Study.

Supplemental Table 2. Summary of Relevant Mutants and Transgenic Plants Used in the Study.

ACKNOWLEDGMENTS

We thank Jeff Dangl (UNC Chapel Hill) for seeds of *RPM1-MYC* transgenic line and María Rosa Ponce (Universidad Miguel Hernández) for seeds of *natb* mutants. E.L. was supported by the Hartmut Hoffmann-Berling International Graduate School, University of Heidelberg. M.W. and R.H. acknowledge funding by the Deutsche Forschungsgemeinschaft (SFB 1036, TP13). We thank the Natural Sciences and Engineering Research Council (Canada) Discovery grant program and the Dewar Cooper Memorial Fund from the University of British Columbia to X.L. for financial support.

AUTHOR CONTRIBUTIONS

F.X., Y.H., C.G., and X.L. designed the experiments and wrote the article. L.L. and S.C. did the MS analysis. P.G. performed the *muse* secondary screen and mapped *muse6* initially. Y.Z. helped with next-generation sequencing data analysis. E.L., M.H., and M.W. performed in vitro acetylation assays. W.B. performed bioinformatics analysis. B.P. assisted with yeast complementation. P.K. analyzed the N termini of all predicted Arabidopsis typical NLR proteins. F.X. and Y.H. performed the rest of the experiments described in the figures. All authors reviewed the article.

Received February 23, 2015; revised April 9, 2015; accepted April 16, 2015; published May 12, 2015.

REFERENCES

Aarts, N., Metz, M., Holub, E., Staskawicz, B.J., Daniels, M.J., and Parker, J.E. (1998). Different requirements for EDS1 and NDR1 by disease resistance genes define at least two R gene-mediated signaling pathways in Arabidopsis. Proc. Natl. Acad. Sci. USA **95:** 10306–10311.

Adam, Z., Frottin, F., Espagne, C., Meinnel, T., and Giglione, C. (2011). Interplay between N-terminal methionine excision and FtsH protease is essential for normal chloroplast development and function in Arabidopsis. Plant Cell **23:** 3745–3760.

Arnesen, T. (2011). Towards a functional understanding of protein N-terminal acetylation. PLoS Biol. **9:** e1001074.

Arnesen, T., Van Damme, P., Polevoda, B., Helsens, K., Evjenth, R., Colaert, N., Varhaug, J.E., Vandekerckhove, J., Lillehaug, J.R., Sherman, F., and Gevaert, K. (2009). Proteomics analyses reveal the evolutionary conservation and divergence of N-terminal acetyltransferases from yeast and humans. Proc. Natl. Acad. Sci. USA **106:** 8157–8162.

Bachan, S., and Dinesh-Kumar, S.P. (2012). Tobacco rattle virus (TRV)-based virus-induced gene silencing. Methods Mol. Biol. **894:** 83–92.

Bachmair, A., Finley, D., and Varshavsky, A. (1986). In vivo half-life of a protein is a function of its amino-terminal residue. Science **234:** 179–186.

Belle, A., Tanay, A., Bitincka, L., Shamir, R., and O'Shea, E.K. (2006). Quantification of protein half-lives in the budding yeast proteome. Proc. Natl. Acad. Sci. USA **103:** 13004–13009.

Bienvenut, W.V., Sumpton, D., Martinez, A., Lilla, S., Espagne, C., Meinnel, T., and Giglione, C. (2012). Comparative large scale characterization of plant versus mammal proteins reveals similar and idiosyncratic N-α-acetylation features. Mol. Cell. Proteomics **11:** M111.015131.

Bienvenut, W.V., Espagne, C., Martinez, A., Majeran, W., Valot, B., Zivy, M., Vallon, O., Adam, Z., Meinnel, T., and Giglione, C. (2011). Dynamics of post-translational modifications and protein stability in the stroma of *Chlamydomonas reinhardtii* chloroplasts. Proteomics **11:** 1734–1750.

Boyes, D.C., Nam, J., and Dangl, J.L. (1998). The *Arabidopsis thaliana* RPM1 disease resistance gene product is a peripheral plasma membrane protein that is degraded coincident with the hypersensitive response. Proc. Natl. Acad. Sci. USA **95:** 15849–15854.

Caesar, R., Warringer, J., and Blomberg, A. (2006). Physiological importance and identification of novel targets for the N-terminal acetyltransferase NatB. Eukaryot. Cell **5:** 368–378.

Cheng, Y.T., Li, Y., Huang, S., Huang, Y., Dong, X., Zhang, Y., and Li, X. (2011). Stability of plant immune-receptor resistance proteins is controlled by SKP1-CULLIN1-F-box (SCF)-mediated protein degradation. Proc. Natl. Acad. Sci. USA **108:** 14694–14699.

Cheng, Y.T., Germain, H., Wiermer, M., Bi, D., Xu, F., García, A.V., Wirthmueller, L., Després, C., Parker, J.E., Zhang, Y., and Li, X. (2009). Nuclear pore complex component MOS7/Nup88 is required for innate immunity and nuclear accumulation of defense regulators in Arabidopsis. Plant Cell **21:** 2503–2516.

Clough, S.J., and Bent, A.F. (1998). Floral dip: a simplified method for Agrobacterium-mediated transformation of Arabidopsis thaliana. Plant J. **16:** 735–743.

Dangl, J.L., Horvath, D.M., and Staskawicz, B.J. (2013). Pivoting the plant immune system from dissection to deployment. Science **341:** 746–751.

Evjenth, R., Hole, K., Karlsen, O.A., Ziegler, M., Arnesen, T., and Lillehaug, J.R. (2009). Human Naa50p (Nat5/San) displays both protein N alpha- and N epsilon-acetyltransferase activity. J. Biol. Chem. **284:** 31122–31129.

Ferrández-Ayela, A., Micol-Ponce, R., Sánchez-García, A.B., Alonso-Peral, M.M., Micol, J.L., and Ponce, M.R. (2013). Mutation of an Arabidopsis NatB N-alpha-terminal acetylation complex component causes pleiotropic developmental defects. PLoS ONE **8:** e80697.

Frottin, F., Martinez, A., Peynot, P., Mitra, S., Holz, R.C., Giglione, C., and Meinnel, T. (2006). The proteomics of N-terminal methionine cleavage. Mol. Cell. Proteomics **5:** 2336–2349.

Frottin, F., Espagne, C., Traverso, J.A., Mauve, C., Valot, B., Lelarge-Trouverie, C., Zivy, M., Noctor, G., Meinnel, T., and Giglione, C. (2009). Cotranslational proteolysis dominates glutathione homeostasis to support proper growth and development. Plant Cell **21:** 3296–3314.

Geissenhöner, A., Weise, C., and Ehrenhofer-Murray, A.E. (2004). Dependence of ORC silencing function on NatA-mediated Nalpha acetylation in *Saccharomyces cerevisiae*. Mol. Cell. Biol. **24:** 10300–10312.

Gibbs, D.J., Bacardit, J., Bachmair, A., and Holdsworth, M.J. (2014a). The eukaryotic N-end rule pathway: conserved mechanisms and diverse functions. Trends Cell Biol. **24:** 603–611.

Gibbs, D.J., Lee, S.C., Isa, N.M., Gramuglia, S., Fukao, T., Bassel, G.W., Correia, C.S., Corbineau, F., Theodoulou, F.L., Bailey-Serres, J., and Holdsworth, M.J. (2011). Homeostatic response to hypoxia is regulated by the N-end rule pathway in plants. Nature **479:** 415–418.

Gibbs, D.J., et al. (2014b). Nitric oxide sensing in plants is mediated by proteolytic control of group VII ERF transcription factors. Mol. Cell **53:** 369–379.

Giglione, C., Vallon, O., and Meinnel, T. (2003). Control of protein life-span by N-terminal methionine excision. EMBO J. **22:** 13–23.

Giglione, C., Serero, A., Pierre, M., Boisson, B., and Meinnel, T. (2000). Identification of eukaryotic peptide deformylases reveals universality of N-terminal protein processing mechanisms. EMBO J. **19:** 5916–5929.

Goetze, S., et al. (2009). Identification and functional characterization of N-terminally acetylated proteins in *Drosophila melanogaster.* PLoS Biol. **7:** e1000236.

Graciet, E., Walter, F., Ó'Maoiléidigh, D.S., Pollmann, S., Meyerowitz, E.M., Varshavsky, A., and Wellmer, F. (2009). The N-end rule pathway controls multiple functions during Arabidopsis shoot and leaf development. Proc. Natl. Acad. Sci. USA **106:** 13618–13623.

Hershko, A., Heller, H., Eytan, E., Kaklij, G., and Rose, I.A. (1984). Role of the alpha-amino group of protein in ubiquitin-mediated protein breakdown. Proc. Natl. Acad. Sci. USA **81:** 7021–7025.

Holman, T.J., et al. (2009). The N-end rule pathway promotes seed germination and establishment through removal of ABA sensitivity in Arabidopsis. Proc. Natl. Acad. Sci. USA **106:** 4549–4554.

Huang, S., Monaghan, J., Zhong, X., Lin, L., Sun, T., Dong, O.X., and Li, X. (2014). HSP90s are required for NLR immune receptor accumulation in Arabidopsis. Plant J. **79:** 427–439.

Huang, Y., Chen, X., Liu, Y., Roth, C., Copeland, C., McFarlane, H.E., Huang, S., Lipka, V., Wiermer, M., and Li, X. (2013). Mitochondrial AtPAM16 is required for plant survival and the negative regulation of plant immunity. Nat. Commun. **4:** 2558.

Huang, Y., Minaker, S., Roth, C., Huang, S., Hieter, P., Lipka, V., Wiermer, M., and Li, X. (2014). An E4 ligase facilitates polyubiquitination of plant immune receptor resistance proteins in Arabidopsis. Plant Cell **26:** 485–496.

Huffaker, R.C., and Peterson, L.W. (1974). Protein turnover in plants and possible means of its regulation. Ann. Rev. Plant Physiolo. **25:** 363–392.

Hwang, C.S., Shemorry, A., and Varshavsky, A. (2010). N-terminal acetylation of cellular proteins creates specific degradation signals. Science **327:** 973–977.

Johnson, K.C., Dong, O.X., Huang, Y., and Li, X. (2012). A rolling stone gathers no moss, but resistant plants must gather their moses. Cold Spring Harb. Symp. Quant. Biol. **77:** 259–268.

Johnston, A.J., Meier, P., Gheyselinck, J., Wuest, S.E., Federer, M., Schlagenhauf, E., Becker, J.D., and Grossniklaus, U. (2007). Genetic subtraction profiling identifies genes essential for Arabidopsis reproduction and reveals interaction between the female gametophyte and the maternal sporophyte. Genome Biol. **8:** R204.

Kim, H.K., Kim, R.R., Oh, J.H., Cho, H., Varshavsky, A., and Hwang, C.S. (2014). The N-terminal methionine of cellular proteins as a degradation signal. Cell **156:** 158–169.

Kim, M.S., et al. (2014). A draft map of the human proteome. Nature **509:** 575–581.

Kim, S.H., Gao, F., Bhattacharjee, S., Adiasor, J.A., Nam, J.C., and Gassmann, W. (2010). The Arabidopsis resistance-like gene SNC1 is activated by mutations in SRFR1 and contributes to resistance to the bacterial effector AvrRps4. PLoS Pathog. **6:** e1001172.

Knuesel, M., Wan, Y., Xiao, Z., Holinger, E., Lowe, N., Wang, W., and Liu, X. (2003). Identification of novel protein-protein interactions using a versatile mammalian tandem affinity purification expression system. Mol. Cell. Proteomics **2:** 1225–1233.

Kozak, M. (1991). Structural features in eukaryotic mRNAs that modulate the initiation of translation. J. Biol. Chem. **266:** 19867–19870.

Lee, S., Liu, B., Lee, S., Huang, S.X., Shen, B., and Qian, S.B. (2012). Global mapping of translation initiation sites in mammalian cells at single-nucleotide resolution. Proc. Natl. Acad. Sci. USA **109:** E2424–E2432.

Li, Y., Li, S., Bi, D., Cheng, Y.T., Li, X., and Zhang, Y. (2010). SRFR1 negatively regulates plant NB-LRR resistance protein accumulation to prevent autoimmunity. PLoS Pathog. **6:** e1001111.

Licausi, F., Kosmacz, M., Weits, D.A., Giuntoli, B., Giorgi, F.M., Voesenek, L.A., Perata, P., and van Dongen, J.T. (2011). Oxygen sensing in plants is mediated by an N-end rule pathway for protein destabilization. Nature **479:** 419–422.

Linster, E., et al. (2015). Down-regulation of N-terminal acetylation triggers ABA-mediated drought responses in Arabidopsis. Nat. Commun., in press.

Liu, C.C., Zhu, H.Y., Dong, X.M., Ning, D.L., Wang, H.X., Li, W.H., Yang, C.P., and Wang, B.C. (2013). Identification and analysis of

the acetylated status of poplar proteins reveals analogous N-terminal protein processing mechanisms with other eukaryotes. PLoS ONE **8:** e58681.

Maekawa, T., Kufer, T.A., and Schulze-Lefert, P. (2011). NLR functions in plant and animal immune systems: so far and yet so close. Nat. Immunol. **12:** 817–826.

Martinez, A., Traverso, J.A., Valot, B., Ferro, M., Espagne, C., Ephritikhine, G., Zivy, M., Giglione, C., and Meinnel, T. (2008). Extent of N-terminal modifications in cytosolic proteins from eukaryotes. Proteomics **8:** 2809–2831.

Meinnel, T., and Giglione, C. (2008). Tools for analyzing and predicting N-terminal protein modifications. Proteomics **8:** 626–649.

Menschaert, G., Van Criekinge, W., Notelaers, T., Koch, A., Crappé, J., Gevaert, K., and Van Damme, P. (2013). Deep proteome coverage based on ribosome profiling aids mass spectrometry-based protein and peptide discovery and provides evidence of alternative translation products and near-cognate translation initiation events. Mol. Cell. Proteomics **12:** 1780–1790.

Miller III, C.A., Martinat, M.A., and Hyman, L.E. (1998). Assessment of aryl hydrocarbon receptor complex interactions using pBEVY plasmids: expressionvectors with bi-directional promoters for use in *Saccharomyces cerevisiae*. Nucleic Acids Res. **26:** 3577–3583.

Palma, K., Zhao, Q., Cheng, Y.T., Bi, D., Monaghan, J., Cheng, W., Zhang, Y., and Li, X. (2007). Regulation of plant innate immunity by three proteins in a complex conserved across the plant and animal kingdoms. Genes Dev. **21:** 1484–1493.

Pechmann, S., Willmund, F., and Frydman, J. (2013). The ribosome as a hub for protein quality control. Mol. Cell **49:** 411–421.

Persson, B., Flinta, C., von Heijne, G., and Jörnvall, H. (1985). Structures of N-terminally acetylated proteins. Eur. J. Biochem. **152:** 523–527.

Polevoda, B., Norbeck, J., Takakura, H., Blomberg, A., and Sherman, F. (1999). Identification and specificities of N-terminal acetyltransferases from *Saccharomyces cerevisiae*. EMBO J. **18:** 6155–6168.

Polevoda, B., Cardillo, T.S., Doyle, T.C., Bedi, G.S., and Sherman, F. (2003). Nat3p and Mdm20p are required for function of yeast NatB Nalpha-terminal acetyltransferase and of actin and tropomyosin. J. Biol. Chem. **278:** 30686–30697.

Rope, A.F., et al. (2011). Using VAAST to identify an X-linked disorder resulting in lethality in male infants due to N-terminal acetyltransferase deficiency. Am. J. Hum. Genet. **89:** 28–43.

Ross, S., Giglione, C., Pierre, M., Espagne, C., and Meinnel, T. (2005). Functional and developmental impact of cytosolic protein N-terminal methionine excision in Arabidopsis. Plant Physiol. **137:** 623–637.

Shemorry, A., Hwang, C.S., and Varshavsky, A. (2013). Control of protein quality and stoichiometries by N-terminal acetylation and the N-end rule pathway. Mol. Cell **50:** 540–551.

Starheim, K.K., Gevaert, K., and Arnesen, T. (2012). Protein N-terminal acetyltransferases: when the start matters. Trends Biochem. Sci. **37:** 152–161.

Starheim, K.K., Arnesen, T., Gromyko, D., Ryningen, A., Varhaug, J. E., and Lillehaug, J.R. (2008). Identification of the human N(alpha)-acetyltransferase complex B (hNatB): a complex important for cell-cycle progression. Biochem. J. **415:** 325–331.

Tasaki, T., Sriram, S.M., Park, K.S., and Kwon, Y.T. (2012). The N-end rule pathway. Annu. Rev. Biochem. **81:** 261–289.

Trujillo, M., and Shirasu, K. (2010). Ubiquitination in plant immunity. Curr. Opin. Plant Biol. **13:** 402–408.

Van Damme, P., Gawron, D., Van Criekinge, W., and Menschaert, G. (2014). N-terminal proteomics and ribosome profiling provide a comprehensive view of the alternative translation initiation landscape in mice and men. Mol. Cell. Proteomics **13:** 1245–1261.

Vanderperre, B., Lucier, J.F., Bissonnette, C., Motard, J., Tremblay, G., Vanderperre, S., Wisztorski, M., Salzet, M., Boisvert, F.M., and Roucou, X. (2013). Direct detection of alternative open reading frames translation products in human significantly expands the proteome. PLoS ONE **8:** e70698.

Varshavsky, A. (2011). The N-end rule pathway and regulation by proteolysis. Protein Sci. **20:** 1298–1345.

Vierstra, R.D. (2009). The ubiquitin-26S proteasome system at the nexus of plant biology. Nat. Rev. Mol. Cell Biol. **10:** 385–397.

Wang, X., Connelly, J.J., Wang, C.L., and Sternglanz, R. (2004). Importance of the Sir3 N terminus and its acetylation for yeast transcriptional silencing. Genetics **168:** 547–551.

Wang, Y., Mijares, M., Gall, M.D., Turan, T., Javier, A., Bornemann, D.J., Manage, K., and Warrior, R. (2010). Drosophila variable nurse cells encodes arrest defective 1 (ARD1), the catalytic subunit of the major N-terminal acetyltransferase complex. Dev. Dyn. **239:** 2813–2827.

Weissman, A.M., Shabek, N., and Ciechanover, A. (2011). The predator becomes the prey: regulating the ubiquitin system by ubiquitylation and degradation. Nat. Rev. Mol. Cell Biol. **12:** 605–620.

Weits, D.A., Giuntoli, B., Kosmacz, M., Parlanti, S., Hubberten, H.M., Riegler, H., Hoefgen, R., Perata, P., van Dongen, J.T., and Licausi, F. (2014). Plant cysteine oxidases control the oxygen-dependent branch of the N-end-rule pathway. Nat. Commun. **5:** 3425.

Wilhelm, M., et al. (2014). Mass-spectrometry-based draft of the human proteome. Nature **509:** 582–587.

Wirtz, M., Heeg, C., Samami, A.A., Ruppert, T., and Hell, R. (2010). Enzymes of cysteine synthesis show extensive and conserved modifications patterns that include N(α)-terminal acetylation. Amino Acids **39:** 1077–1086.

Xu, F., Xu, S., Wiermer, M., Zhang, Y., and Li, X. (2012). The cyclin L homolog MOS12 and the MOS4-associated complex are required for the proper splicing of plant resistance genes. Plant J. **70:** 916–928.

Xu, F., Kapos, P., Cheng, Y.T., Li, M., Zhang, Y., and Li, X. (2014). NLR-associating transcription factor bHLH84 and its paralogs function redundantly in plant immunity. PLoS Pathog. **10:** e1004312.

Yen, H.C., Xu, Q., Chou, D.M., Zhao, Z., and Elledge, S.J. (2008). Global protein stability profiling in mammalian cells. Science **322:** 918–923.

Zhang, Y., Goritschnig, S., Dong, X., and Li, X. (2003). A gain-of-function mutation in a plant disease resistance gene leads to constitutive activation of downstream signal transduction pathways in suppressor of npr1-1, constitutive 1. Plant Cell **15:** 2636–2646.